

# Orbital Angular Momentum Waves: Generation, Detection and Emerging Applications

Rui Chen, *Member, IEEE*, Hong Zhou, Marco Moretti, *Member, IEEE*, Xiaodong Wang, *Fellow, IEEE*, and Jiandong Li, *Senior Member, IEEE*

**Abstract**—Orbital angular momentum (OAM) has aroused a widespread interest in many fields, especially in telecommunications due to its potential for unleashing new capacity in the severely congested spectrum of commercial communication systems. Beams carrying OAM have a spiral wavefront phase structure and a field strength with a singularity along the axial center, which can be used for particle manipulation, imaging and information transmission. The number of orthogonal OAM modes in a single beam is theoretically infinite and each mode is an element of a complete orthogonal basis that can be employed for multiplexing different signals, thus greatly improving the spectrum efficiency. In this paper, we comprehensively summarize and compare the methods for generation and detection of optical OAM, radio OAM and acoustic OAM. Then, we represent the applications and technical challenges of OAM in communications, including free-space optical communications, optical fiber communications, radio communications and acoustic communications. To complete our survey, we also discuss the state of art of particle manipulation and object imaging with OAM beams.

**Index Terms**—Orbital angular momentum (OAM), optical, radio, acoustic, vortex, generation, detection, communications, particle manipulation, imaging.

## I. INTRODUCTION

**E**lectromagnetic waves carry both energy and momentum, where momentum comprises linear momentum  $P$  and angular momentum  $L$ . In particular, angular momentum has an additive component linked to polarization, *spin angular momentum* (SAM), and another one associated with spatial distribution, which is called *orbital angular momentum* (OAM). The relationship between SAM and OAM can be explained referring to the model of electron rotation around the nucleus: the momentum generated by the circular motion of electrons around the nucleus is equivalent to OAM, and the momentum generated by the spin of electrons is equivalent to SAM.

In 1992, Allen et al. first combined the concept of OAM with the idea of *optical vortex* [1]: in an optical vortex the planes of constant phase of the electric and magnetic vector fields form a corkscrew or helicoid running in the direction of propagation. The vortex is characterized by a number, called the *topological charge*, which indicates the number of twists the light does in one wavelength. The larger the number of

twists, the faster the light is spinning around the axis. Accordingly, the OAM carried by the optical vortex theoretically has an infinite number of eigenstates and is defined in an infinite-dimensional Hilbert vector space. Because of this, the application potentials of OAM in the field of communications are enormous, even, as we will see, there are still some problems to be solved before a full deployment. If the OAM dimension of photons can be fully utilized for information modulation or multiplexing, the information capacity of a single photon can be significantly improved, thereby leading to an increase of the transmission capacity of single-wavelength and single-mode fibers. In addition, since the vortex beam has a helical wavefront, its axial center field in the direction of propagation is null, creating the potential for applications in particle manipulation and optical imaging.

The potentials of employing OAM for communications are not restricted to electromagnetic waves at light frequencies. In 2007, Thide et al. [2] proposed to apply the concept of optical vortex to the field of wireless communications, i.e., in a range of lower radio frequencies than light. Moreover, a different line of research has showed that, unlike electromagnetic waves, sound waves do not have polarization or spin effects and cannot carry SAM but only carry OAM. Although the concept of acoustic vortex was first proposed in 1979 [3], twenty years later, Hefner and Marston [4] derived the relationship between sound pressure and angular momentum, perfecting the theory of the *acoustic vortex*. The application of OAM to wireless communications and acoustic communications, especially underwater communications, is expected to open new fields of research and possibly break the limits of existing communication systems.

The rest of this paper is organized as follows: Section II summarizes the common methods of producing optical OAM, radio OAM, and acoustic OAM. OAM detection methods are introduced and compared in Section III. In Section IV, the research progress and challenges of OAM in communication systems are highlighted. Section V discusses the application of OAM to particle manipulation and imaging. Conclusions are drawn in Section VI.

## II. GENERATION OF OAM WAVES

Since Allen et al. in 1992 proved that the optical vortex with a spiral wavefront carries OAM, the research on OAM has gradually deepened and broadened. A variety of methods for generating OAM have been proposed in the fields of light waves, electromagnetic waves, and sound waves.

Rui Chen, Hong Zhou and Jiandong Li are with the State Key Laboratory of ISN, Xidian University, Shaanxi 710071, China (e-mail: rchen@xidian.edu.cn, hzhou\_l@stu.xidian.edu.cn, jdli@mail.xidian.edu.cn). Rui Chen is also with State Key Laboratory of Rail Transit Engineering Informatization (FSDI).

Marco Moretti is with the University of Pisa, Dipartimento di Ingegneria dell'Informazione, Italy (e-mail: marco.moretti@iet.unipi.it).

Xiaodong Wang is with the Electrical Engineering Department, Columbia University, New York, NY 10027 USA (e-mail: wangx@ee.columbia.edu).

### A. Optical OAM

In optics, the vortex beam can be either directly output by the laser cavity, or a Gaussian beam can be converted into a vortex beam by a converter, such as a cylindrical lens, a spiral phase plate, a phase hologram, a super surface material or a q-plate. The simplest example of a light beam carrying OAM is a beam with a phase in the transverse plane of  $\exp(i\ell\phi)$ , where  $\phi$  is the azimuthal angle with respect to the beam axis and  $\ell$ , called the topological charge or OAM mode, can be any integer value, positive or negative. Helically phased beams carry an OAM corresponding to a value of  $\ell\hbar$  per photon [5], where  $\hbar$  is the Planck's constant.

Even before Allen showed that the vortex beam carries OAM, research has been focused on vortex beams and on how to generate them. In [6], the resonance phenomenon is exploited to generate a vortex from an optical cavity. The laser cavity normally produces a mixture of multiple modes including the basic mode. By placing a component inside the laser cavity, such as a spot-defect mirror [7], the laser cavity can be forced to resonate on a specific OAM mode.

In [1], [8], *cylindrical lenses* are used to transform a Hermite-Gaussian (HG) laser beam into a helically-phased Laguerre-Gaussian (LG) beam. An example of a 2nd order HG mode decomposition and LG mode synthesis is shown in Fig. 1 (a). The  $45^\circ$  angle HG mode can be decomposed into a series of HG modes, and this series of HG modes can be rephased to obtain the LG mode. This rephasing can be achieved by changing the Gouy phase shift in the HG mode. Two cylindrical lens mode converters, the  $\pi/2$ -converter and the  $\pi$ -converter, are proposed in [8], as shown in Fig. 1 (b). The functions of the mode converters are similar to the polarization of birefringence  $\lambda/4$  and  $\lambda/2$  plates. The  $\pi/2$ -converter can convert a HG mode with indices  $m, n$ , oriented at  $45^\circ$  angle to the lens axis, into a LG mode with topological charge  $\ell = m - n$  and number of radial nodes in the intensity distribution  $p = \min(m, n)$ . The  $\pi$ -converter changes the index of the input mode, that is,  $HG_{m,n}$  turns into  $HG_{n,m}$  or  $LG_{m,n}$  turns into  $LG_{n,m}$ , which has an azimuthal dependence of the opposite sign. Cylindrical lens mode converters have high conversion efficiency and generate OAM with high purity, but they require high construction precision, and, at the same time, have poor flexibility because they require a very precise incident field angle.

The *spiral phase plate* (SPP) is another way to implement the vortex beam [9]. As shown in Fig. 2, the SPP is designed like a rotating step so that its thickness increases as the azimuth angle increases but is uniform radially. The step height is expressed as  $S = \ell\lambda\theta/[2\pi(n - n_0)]$ , where  $n$  is the refractive index of the transparent dielectric material of the plate,  $n_0$  is the refractive index of the external medium,  $\ell$  is the topological charge,  $\lambda$  is the wavelength of the incident light, and  $\theta$  is the spatial azimuth. When a plane wave of Gaussian light passes through the phase plate, the light beam experiences a different phase in the azimuth direction due to the spiral thickness of the phase plate and is converted into a helically phased beam with topological charge  $\ell$ . SPP has high conversion efficiency and can be used for high power laser beams but has also the

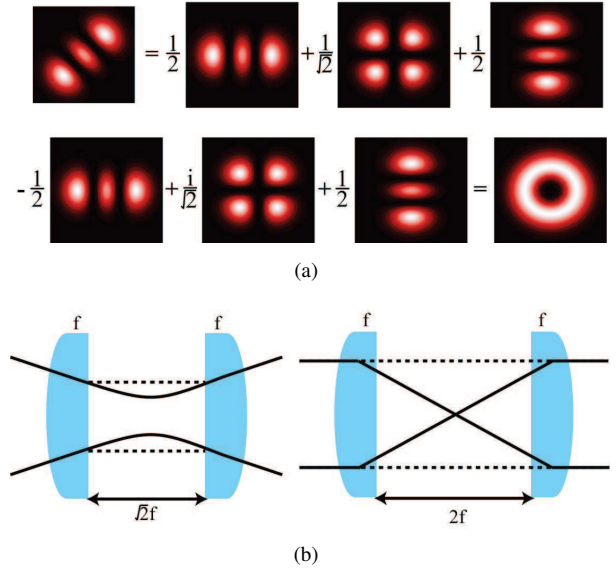


Fig. 1: (a) An example of 2nd order HG mode decomposition and LG mode synthesis; (b)  $\pi/2$ -converter and  $\pi$ -converter [5].

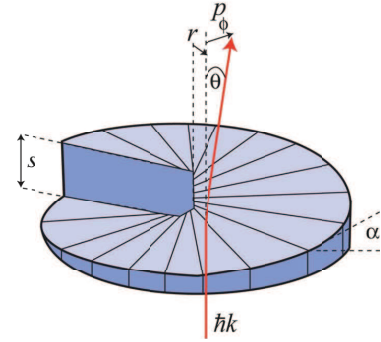


Fig. 2: Schematic diagram of SPP [5].

limit that it can generate a single mode only and it has very tight precision requirements.

Instead of producing a complex refractive optical element to generate a vortex wave, one can employ a computer-generated hologram to design a diffractive optical element whose transmittance function is related to the spiral phase  $\exp(i\ell\phi)$ . *Holographic diffraction gratings*, such as Fresnel spiral diffraction gratings and  $\ell$ -fold forked diffraction gratings [10]–[12], are generated by using a photolithographic process to record an interference pattern on a photoresist-coated substrate. When Gaussian light is incident on the  $\ell$ -fold forked diffraction grating, a vortex beam having a topologically charged  $n\ell$  mode can be obtained at the  $n$ th diffraction order. Holographic diffraction gratings are relatively simple and fast to produce and provide good wavefront flatness and high efficiency for a single polarization plane. However, as the number of diffraction orders increases, the quality of the vortex beam is seriously degraded and this method is generally only used to generate low-order vortex beams.

Unlike the SPP and the diffraction grating described above,

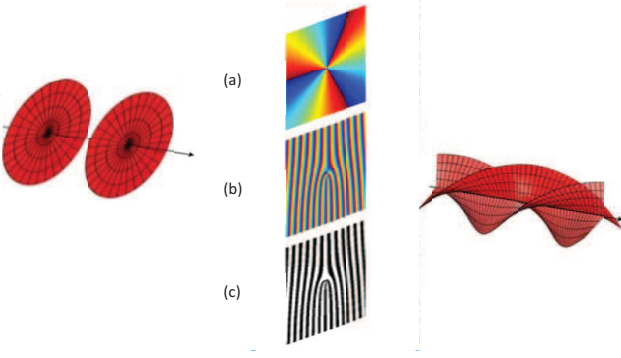


Fig. 3: (a) Phase hologram in the form of a spiral phase hologram; (b) Phase hologram in the form of an  $\ell$ -fold forked hologram; (c) Phase hologram in the form of a binarized  $\ell$ -fold forked grating.

the *spatial light modulator* (SLM) can generate vortex beams with different topological charges [13], [14]. A SLM is a pixelated liquid crystal device whose liquid crystal molecules can be programmed to dynamically change the incident beam parameters, including the beam phase in the transverse plane, to create a vortex beam. In detail, a phase hologram with a transmittance function of  $\exp(i\ell\phi)$  is digitally generated and loaded on the SLM so that the SLM will determine the phase of each point in the two-dimensional space according to the value of each pixel of the input phase hologram. In general, to generate a vortex beam the phase hologram loaded onto the SLM is in the form of: a) a spiral phase hologram, b) a  $\ell$ -fold forked hologram, and c) a binarized  $\ell$ -fold forked grating (shown in Figs. 3(a), 3(b), and 3(c), respectively). The spiral phase hologram produces a vortex beam with only a single topological charge and exits vertically. The forked hologram can control the exit direction of the vortex beam, while the binarized forked grating has multiple diffraction orders, which produce different topological charges at different diffraction orders. Liquid crystal SLM are very flexible since they can control various parameters of the vortex beam but they are relatively expensive and have an energy threshold that makes their use impossible with high power laser beams. Recently, in addition to the liquid crystal SLM, a diffractive optical element using a digital micro-mirror device (DMD) has been introduced [15], [16]. In contrast to the liquid crystal device, DMD cost less and are faster but their diffraction efficiency is lower.

Transformation optics is a recently developed discipline that employs complex artificial materials, called *metamaterials*, to make transformations in optical space. Generation of optical OAM is one of the fields where the findings of transformation optics can be applied: the metamaterials are planar ultra-thin optical components, usually composed of sub-wavelength constitutional units, such as V-shaped antennas [17], [18], as shown in Fig. 4, L-shaped antennas [19], rectangular apertures [20], and rectangular split-ring resonators [21]. Rather than relying on the continuous transitions of conventional optics, these planar ultra-thin optical components operate by forcing a sudden change of beam phase, amplitude or polarization at

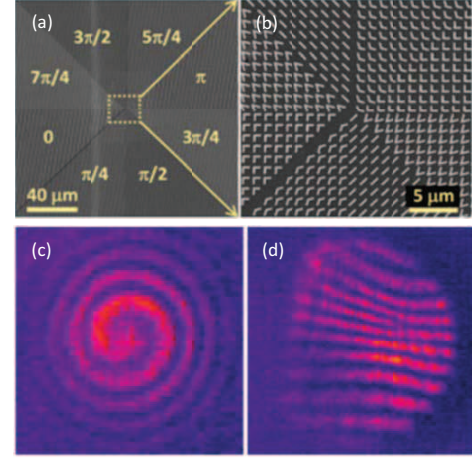


Fig. 4: (a) The metamaterial is composed by a sub-wavelength V-shaped antenna array; (b) Partially enlarged view; (c) Interference pattern of the vortex beam with  $\ell = 1$  and a co-propagating Gaussian beam; (d) Interference pattern of the vortex beam with  $\ell = 1$  and a Gaussian beam when the two are tilted with respect to each other [17].

the interface. Thus, optical OAM is obtained by controlling the geometrical parameters (shape, size, direction, etc.) of the metamaterial to manipulate the phases of different azimuths and change the spatial phase of the incident light. As shown in Fig. 4, the metamaterial structure is composed by a sub-wavelength V-shaped antenna array, and the beam phase can be controlled by adjusting the angle between the two arms of the V-shaped antenna. The entire surface is divided into eight regions, and the phase difference between the adjacent regions is  $\pi/4$ . This object generates a helical phase shift with respect to the front of the incident beam producing a vortex with topological charge of  $\ell = 1$ . The biggest advantage of the use of metamaterials is their small size that allows for easy integration. Unfortunately, only a vortex beam with a particular topological charge can be generated by a single device.

The *q-plate* [22], [23] is a liquid crystal panel that has a uniform birefringence phase retardation  $\delta$  and a transverse optical axis pattern with nonzero topological charge. The angle between the optical axis orientation and the  $x$ -axis in  $xy$  plane can be expressed as  $\alpha(r, \phi) = q\phi + \alpha_0$ , where  $\alpha_0$  is an initial optical axis orientation. Q-plate patterns with different values of  $q$  and  $\alpha_0$  are shown in Fig. 5. When *q-plate* is optimally tuned, i.e.  $\delta = \pi$ , a light beam incident on it is modified to have a topological charge variation  $\Delta\ell = \pm 2q$ . For example a circularly polarized Gaussian passing through a tuned *q-plate* with  $q = 1$  has a helical wavefront with topological charge  $\ell = \pm 2$ , where the sign depends on the chirality of the input polarized light, as shown in Fig. 5(e). The characteristic of *q-plates* is that they generate OAM as a result of optical spin-to-orbital angular momentum conversion, exploiting the law of conservation of angular momentum. The *q-plate* is essentially a Pancharatnam-Berry phase optic component that controls the wavefront shape by transitioning the polarization state. In addition to the *q-plate*, the computer-generated sub-wavelength dielectric grating [24], [25] and the L-shaped antenna array

TABLE I: Comparison of Optical OAM Generation Methods.

Features	Cylindrical lenses	SPPs	Holographic gratings	SLMs	Metamaterials	Liquid crystal $q$ -plates
<b>Cost</b>	Normal	Low	Low	High	Low	High
<b>Speed</b>	Normal	Normal	Fast	Normal	Normal	Fast
<b>Conversion efficiency</b>	High	High	Low	Normal	Relatively high	Relatively high
<b>OAM mode</b>	Multiple modes; Pure mode	Single mode; Non-pure mode	Single mode; Composite mode	Multiple modes; Composite mode	Single mode	Single mode; Pure mode
<b>Working frequency</b>	All	One point	All	All	A range	All
<b>Processing difficulty</b>	High	High	High	Low	High	Low
<b>System complexity</b>	High	Low	Low	High	Low	Low

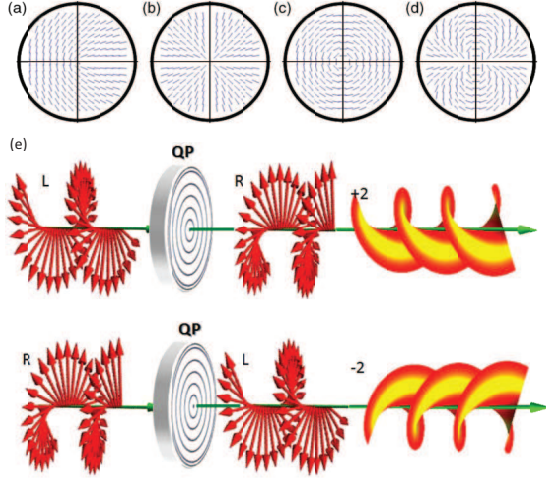


Fig. 5: Four examples of  $q$ -plate patterns with: (a)  $(q, \alpha_0) = (1/2, 0)$ , (b)  $(q, \alpha_0) = (1, 0)$ , (c)  $(q, \alpha_0) = (1, \pi/2)$  and (d)  $(q, \alpha_0) = (2, 0)$ ; (e) Pictorial illustration of the optical action of a tuned  $q$ -plate on an input circularly polarized plane-wave light [22].

metamaterial proposed in [19] are also Pancharatnam-Berry optical device. The  $q$ -plate is capable of producing a pure OAM mode but, being made of liquid crystal, has also an energy threshold and thus cannot be used in conjunction with high power laser beams.

Table I compares the common methods of producing optical OAM from multiple dimensions. The simplicity of the SPP and the flexibility of the SLM make them widely used. Metamaterials are often used in small integrated vortex beam emitters.

### B. Radio OAM

OAM is a fundamental characteristic of electromagnetic waves at all frequencies and is not limited to the optical band and can be generated in the radio band as well as in the audio band.

In analogy with the generation of optical OAM, SPPs, whose thickness increases with the increase of the azimuth angle, have been the first method used to generate OAM [32],

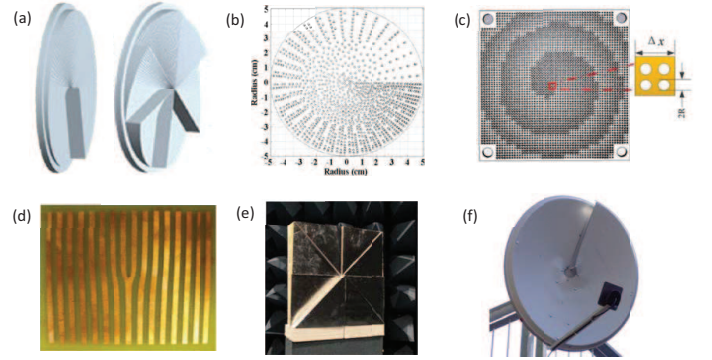


Fig. 6: (a) Single-stage and multi-stage SPPs [26]; (b) and (c) Planar SPPs [27], [28]; (d) Forked gratings [29]; (e) Stepped spiral reflecting surface [30]; (f) Spiral parabolic antenna [31].

[33] at high radio frequencies. To generate a high-order vortex beam, the spiral surface is usually replaced by a stepped surface to form a stepped SPP [26] as shown in Fig. 6 (a). Recently, also planar SPPs [27], [28] have been proposed for generating radio OAM. Unlike conventional SPPs, which use thickness to change the beam phase, planar phase plates adjust the wavefront of the electromagnetic wave by controlling the change in dielectric constant using different borehole densities [27] or radius [28]. Although these devices have a planar structure, like ordinary phase plates, the requirements in terms of structural precision is very high and the plate is difficult to manufacture.

To create OAM, the stepped spiral surface can be also built as a reflector illuminated by a conventional antenna [30]. The *spiral reflector* causes the reflected electromagnetic wave to have a wave path difference at different positions of the cross section, so that the desired electromagnetic vortex is created. As in Fig. 6 (e), the reflecting stepped spiral surface is divided into  $N$  discrete regions, each of which introduces a discontinuous phase difference  $2\pi/N$ . The topological charge of radio OAM of stepped surfaces is  $\ell = 2\mu_0(N+1)/(\lambda N)$ , where  $N$  is the number of regions into which the reflection surface is partitioned,  $\mu_0$  is the total surface spacing, and  $\lambda$  is the wavelength of the incident electromagnetic wave. When  $N$  tends to infinity, the stepped spiral reflector becomes a



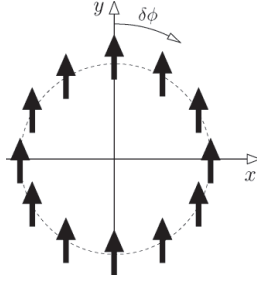


Fig. 7: Schematic diagram of UCAA [2] .

continuous form, such as the spiral parabolic antenna used in the 2012 OAM wireless communication experiment [31]. The spiral reflector is simple and easy to implement. However, it can only respond to specific frequencies and the OAM mode produced by this method is difficult to determine.

*Holographic gratings* designed by means of computer-generated holograms are also a method of generating radio OAM in analogy with the generation method at optical frequencies [29].

Nevertheless, *uniform circular antenna array* (UCAA), as in Fig. 7, is the most commonly used method for generating electromagnetic vortex [2], [34]. The UCAA is composed by  $N$  elements, uniformly distributed on the circumference. Each array element is controlled by an input signal of the same amplitude but different phase and the phase difference between adjacent array elements is  $\Delta\phi = 2\pi\ell/N$ , where  $\ell$  is the OAM mode, so that the phase difference over the whole array is  $2\pi\ell$ . Theoretically, an UCAA with  $N$  array elements can produce a distortion-free vortex wave with  $|\ell| < N/2$ . UCAA can be used in different forms of antennas, such as dipole antenna [2], [34], Vivaldi antenna [35], horn antenna [36], Yagi antenna [37], and microstrip patch antenna [38], [39]. Radio OAM generation with imperfect uniform circular arrays (IUCA) is discussed in [40]. In [41] a circular time switched array (TSA) is employed to generate vortex electromagnetic waves. This TSA method uses high-speed RF switches to activate the array elements sequentially, enabling the simultaneous generation of all OAM modes at the harmonic frequencies of the TSA switching cycle. The mode of the electromagnetic vortex generated by the UCAA can be controlled flexibly, but this usually requires a complicated feed network.

Similar to the generation method at optical frequencies, *metamaterials*, which can be classified as reflective metamaterials [42]–[46] and transmissive metamaterials [47], are also used to generate vortex electromagnetic waves. The schematic diagram of generating OAM using a reflective metamaterial is shown in Fig. 8, where the incident wave at radio frequencies is reflected and converted into a vortex wave.

In addition to metamaterials, also *q-plates*, made by carving a series of concentric rings on a dielectric plate, can be used to generate a vortex wave at radio frequencies [48].

Table II compares the common methods of generating vortex at radio frequencies. SPPs and holographic gratings are suitable for the generation of vortex at high frequencies and even millimeter-waves, spiral reflectors and UCAAs are

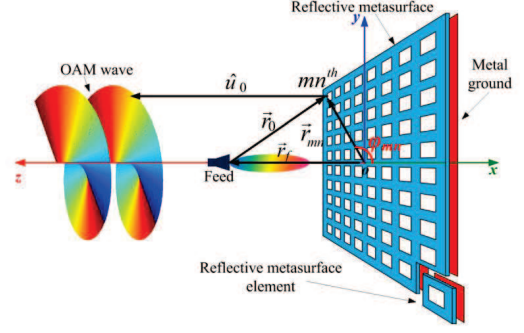


Fig. 8: Schematic diagram of producing OAM with a reflective metamaterial [43].

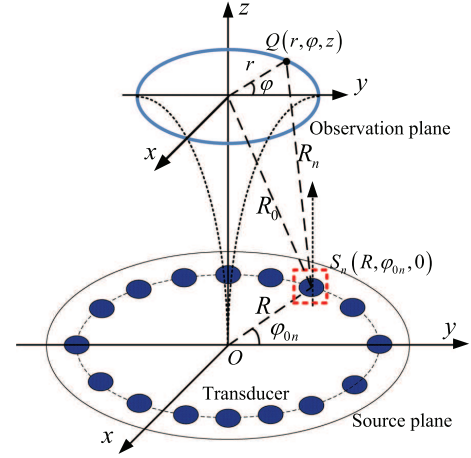


Fig. 9: Schematic diagram of a UCTA [53].

suitable for the generation of a vortex wave at low frequencies, and metamaterials are expected to be used in miniaturized integrated circuits.

### C. Acoustic OAM

OAM has found applications in audio bands as well. Because of their simple structure and high conversion efficiency, SPPs are widely used to generate optical vortex and radio vortex. Similarly, SPPs have also been employed to generate acoustic vortex. The acoustic SPP in [49] has thickness  $h$  that varies with azimuth,  $h = \ell\theta/[2\pi f(c_0^{-1} - c^{-1})]$ , where  $c_0$  is the sound speed in the surrounding medium,  $c$  is the sound speed in the phase plate, and  $f$  is the frequency of the incident wave. Another absorbing SPP using optoacoustic technology was proposed in 2004 to generate OAM in the ultrasonic band [50]. The difference is that the optoacoustic conversion efficiency of this SPP is very low, and this device requires high-energy short pulse excitation. In addition to passive SPP, active sound source with spiral thickness [51], [52] are used to generate acoustic vortices. The dimensions of those spiral structures is generally dozens of wavelengths and their large volume limits the application in low frequency sound waves.

In analogy with antenna arrays in electromagnetic vortex, transducer arrays, especially *uniform circular transducer arrays* (UCTAs), are also widely used to generate acoustic vor-

TABLE II: Comparison of Radio OAM Generation Methods.

Features	SPPs	Holographic gratings	Spiral reflectors	UCAAs	Metamaterials	Dielectric $q$ -plates
<b>Cost</b>	Low	Low	Low	High	Low	Low
<b>Speed</b>	Normal	Fast	Normal	Normal	Fast	Normal
<b>Conversion efficiency</b>	High	Low	Normal	Normal	Relatively high	/ (Not discussed)
<b>OAM mode</b>	Single mode; Non-pure mode	Single mode	Single mode; Non-pure mode	Multiple modes; Composite mode	Single mode	Single mode; Pure mode
<b>Working frequency</b>	One point	All	One point	All	One point	One point
<b>Processing difficulty</b>	High	High	High	Low	High	High
<b>System complexity</b>	Low	Low	Low	High	Low	Low

tices carrying OAM. A simple four-panel transducer has first been proposed to produce acoustic vortices [4]. Subsequently, hexagonal arrays [54] and UCTAs [53], [55], [56] have also been studied: UCTAs use fewer transducers than hexagonal arrays, and, by adjusting the phase difference between adjacent transducers, are capable to flexibly generate acoustic vortices with different OAM modes. Fig. 9 shows a UCTA composed by  $N$  uniformly spaced elements: by driving each transducer with a sine wave with frequency  $f$  and phase difference  $\Delta\varphi = 2\pi\ell/N$ , the array can generate an acoustic vortex with  $|\ell| \leq \lfloor (N-1)/2 \rfloor$ , where  $\lfloor x \rfloor$  indicates the greatest integer less than or equal to  $x$ . By precisely controlling the amplitude and the phase of the excitation signals, UCTAs can generate multiplexed acoustic vortices. Since the transducers size is comparable to the acoustic wavelengths, it should be noted that each transducer can be regarded as a point source at low frequencies, but the directivity of the source needs to be considered in high frequency acoustic fields. Like UCAAs, UCTAs also require complex control circuits, and the complexity grows with the number of transducers.

Another method for generating acoustic vortex is to employ sub-wavelength *spiral diffraction gratings* depicted on rigid materials, which, due to the diffraction effect, can generate acoustic vortices in the paraxial region. Higher mode acoustic OAM can be produced by increasing the number of arms of spiral gratings. Using a grating with  $m$  arms, an acoustic vortex with a topological charge of  $\ell = mn$  is obtained at the  $n$ th diffraction order. Spiral gratings can be designed as Archimedes spiral type [57], [58], Fresnel spiral type [59], and logarithmic spiral type [60], as shown in Fig. 10. The first two types can only be used for a specific frequency, while the logarithmic spiral is for a wider frequency range. In polar coordinates, when  $m = 1$  the two concentric logarithmic spirals are denoted as  $r_1 = a_1 \exp(b\theta)$  and  $r_2 = a_2 \exp(b\theta)$ , respectively, where  $\theta$  is the angular coordinate,  $r_1$  and  $r_2$  are the radial coordinates,  $a_1$  and  $a_2$  are the inner radii of the two spirals,  $b$  varies with the number of arms, determining the growth rate of the spiral and the width of the spiral grating is  $d = r_2 - r_1$ . As long as the wavelength of the incident acoustic wave is greater than  $2d_{min}$  and less than  $2d_{max}$ , effective diffraction can occur to obtain the desired acoustic OAM. Such a passive spiral diffraction grating has

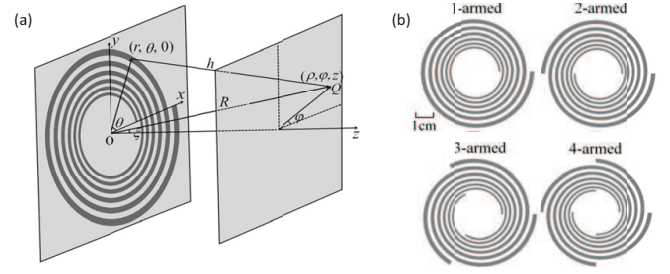


Fig. 10: (a) Diagram of the working principle of the multi-arm coiling slits for generating the stable acoustic vortices; (b) Summary of the schematic of the one-armed, two-armed, three-armed, and four-armed coiling slits [60].

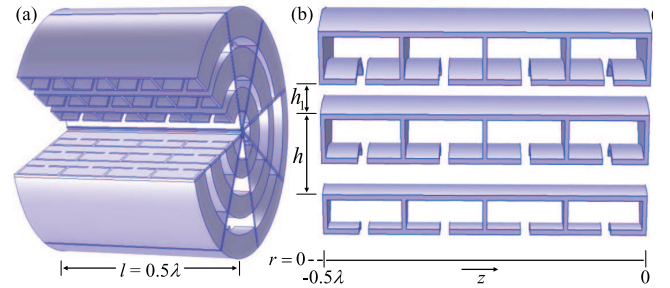


Fig. 11: (a) Schematic of the assembled layer consisting of eight fanlike sections of resonators; (b) An individual section consisting of three rows of resonators in the radial  $r$  direction, sided by pipes of varying height  $h_1$  to produce the needed effective wave number [62].

a low diffraction efficiency. Recently, an active spiral grating fabricated using a cellular ferroelectret film has been proposed to improve diffraction efficiency [61].

In addition to optical OAM and radio OAM, *metamaterial* can also be used to generate acoustic OAM [62]–[64]. Usually, to generate acoustic OAM a metasurface with a sub-wavelength thickness is equally divided into  $N$  regions. By changing structural parameters in each region, the phase of the outgoing acoustic wave can be adjusted to be spirally distributed along the azimuthal direction. A planar metamaterial structure for converting planar acoustic waves into vortex

TABLE III: Comparison of Acoustic OAM Generation Methods.

Features	SPPs	UCTAs	Spiral diffraction gratings	Metamaterials
<b>Cost</b>	Low	High	Low	Low
<b>Speed</b>	Normal	Normal	Normal	Normal
<b>Conversion efficiency</b>	High	Normal	Low	Relatively high
<b>OAM mode</b>	Single mode; Non-pure mode	Multiple modes; Composite mode	Multiple modes	Single mode
<b>Working frequency</b>	One point	All	A range	One point
<b>Processing difficulty</b>	High	Low	High	High
<b>System complexity</b>	Low	High	Low	Low

acoustic waves using acoustic resonance is shown in Fig. 11. The metamaterial is divided into eight fanlike sections. Each individual section is configured to be composed of three rows of resonators in the radial direction. Each row consists of four Helmholtz cavities and a straight pipe. The phase of the outgoing sound wave can be expressed as  $\phi_{out} = \phi_{in} + k^{(eff)}l$ , where  $k^{(eff)}$  is the equivalent wave number and varies with the ratio of the heights of the pipe and resonator  $h_1/h$  and  $l$  is the structural thickness. It can be shown that when  $k^{(eff)}$  depends on azimuth change, the output phase also changes with azimuth. The cascade of four Helmholtz cavities in each row can flexibly control  $k^{(eff)}$  from  $-k$  to  $k$  over the whole azimuth, ie, achieving an exit phase from 0 to  $2\pi$ , while the combination of the Helmholtz cavity and the straight pipe can get a very high transmittance. The phase difference between adjacent sections of the metamaterial is  $\pi/4$ , so that planar acoustic waves are converted into vortex sound waves with a topological charge of  $\ell = 1$ . This metamaterial structure has the advantages of being highly efficient with a small size and a planar shape. However, the proposed structure can only be used for the generation of acoustic vortices at specific frequencies in the air.

Table III compares the generation methods of acoustic OAM. The UCTA is the most flexible and fast method, and is widely used as an underwater acoustic vortex generator.

#### D. Summary

Table IV summarizes the common methods of generating OAM. Optical, radio and acoustic vortices can carry OAM. Methods to generate optical vortex beams have been developed relatively earlier with respect to the others and many radio OAM and acoustic OAM generation methods, such as SPP and metamaterials, are proposed by analogy with the generation of optical OAM. Based on their respective characteristics, special methods have been proposed to produce radio OAM and acoustic OAM, such as UCAs and UCTAs.

### III. DETECTION OF OAM WAVES

At the receiver side, different OAM modes can be separated easily by exploiting the orthogonality of the spiral wavefronts. A variety of methods for detecting OAM have been proposed

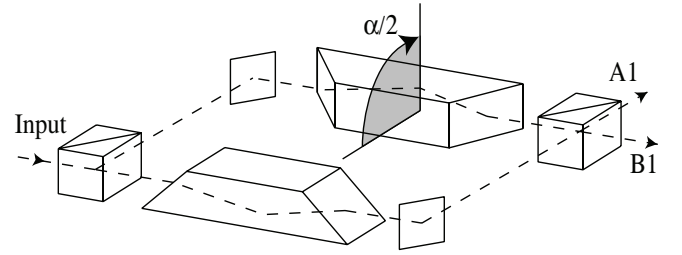


Fig. 12: A Mach-Zehnder interferometer with a Dove prism placed in each arm [65].

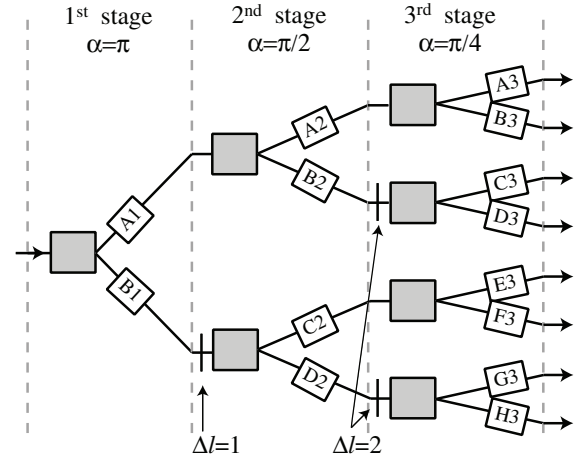


Fig. 13: The first three stages of a general sorting scheme [65].

for light and radio waves. In the acoustic frequency range, OAM detection is still in its early days.

#### A. Optical OAM

Being the detection of optical OAM the inverse process of generating OAM, OAM modes can be detected by using an *inverse SPP* designed for the specific mode to be detected. Moreover, a vortex beam with a topological charge of  $\ell$  is converted into planar Gaussian light after being irradiated through a *holographic grating* [66] with a transmittance function related to the anti-helical phase factor  $\exp(-i\ell\theta)$ . Using spatial mode filters, Gaussian light can be separated from other

TABLE IV: Summary of OAM Generation Methods.

Methods	Introduction and Features	Remarks
<b>Cylindrical lenses</b>	HG mode without OAM can be converted to LG mode with OAM. High conversion efficiency; high OAM mode purity; the special incident field is required.	Optical OAM
<b>SPPs</b>	With spiral thickness $h = \ell\lambda\theta/[2\pi(n - n_0)]$ in optics and electromagnetics and $h = \ell\theta/[2\pi f(c_0^{-1} - c^{-1})]$ in acoustics. Simple structure; high precision; high conversion efficiency; specific working frequency.	Optical OAM Radio OAM Acoustic OAM
<b>Holographic gratings</b>	Interference patterns of plane waves and vortex waves, such as $\ell$ -fold fork diffraction gratings, whose transmittance function is related to $\exp(i\ell\theta)$ . Simple and fast; low diffraction efficiency.	Optical OAM Radio OAM
<b>SLMs</b>	A pixelated liquid crystal device loaded with a phase hologram whose transmittance function related to $\exp(i\ell\theta)$ . High cost; flexible control.	Optical OAM
<b>UCAAs</b>	$N$ elements uniformly distributed on the circumference with the excitation phase difference is $2\pi\ell/N$ can generate radio OAM with $ \ell  < N/2$ . Flexible control; a complicated feed network is required.	Radio OAM
<b>UCTAs</b>	Similar to UCAAs.	Acoustic OAM
<b>Spiral reflectors</b>	The reflection surfaces are divided into $N$ discrete regions and can generate OAM with $\ell = 2\mu_0(N + 1)/(\lambda N)$ . Simple structure; beam convergence effect; it is difficult to determine topological charge values; specific working frequency.	Radio OAM
<b>Spiral diffraction gratings</b>	Archimedes spiral type, Fresnel spiral type or logarithmic spiral type gratings depicted on sub-wavelength rigid materials. Low diffraction efficiency; the topological charge is changed by controlling the number of arms of the grating.	Acoustic OAM
<b>Metamaterials</b>	It is composed of sub-wavelength constitutional units and can flexibly manipulate wavefront phase, amplitude and polarization. Low cost; small size; easy integration; high conversion efficiency; specific working frequency.	Optical OAM Radio OAM Acoustic OAM
<b>Q-plates</b>	A uniform birefringent liquid crystal or dielectric plate that can generate OAM as a result of optical spin-to-orbital angular momentum conversion. High conversion efficiency; fast response; high OAM mode purity; simple chiral control of OAM beams.	Optical OAM Radio OAM

OAM beams, detecting only one specific OAM mode at the time. For multiplexed OAM modes, a series of holographic gratings are required to sequentially detect each single OAM mode, or, alternatively, it can be used a beam splitter for parallel detection. In [67] and [68] a two-dimensional forked holographic grating, which is the superposition of a vertical grating and a horizontal grating, is designed to simultaneously detect 8 OAM modes. Two-dimensional Dammann gratings, combining the characteristics of conventional gratings and Dammann gratings, can achieve equal energy distribution on the designed diffraction order, expanding the detection range of the grating [69], [70]. At present, Dammann holographic gratings are widely used at the receive end of optical communication systems since they can perform parallel detection on multiple OAM states. These holographic gratings require high

precision and are normally loaded onto a SLM or recorded using advanced grating fabrication techniques. At the same time, their conversion efficiency is not higher than  $1/N$ , where  $N$  is the total number of detected modes. Recently, in [71] has been proposed a novel phase hologram, designed by modifying the Lin's algorithm [72], which can be used to achieve almost complete concentration of incident energy to a specified target OAM state that can be detected more effectively than with conventional forked grating.

A vortex wave with topological charge of  $\ell$  can interfere with a plane wave to obtain  $\ell$  spiral stripes or  $\ell$ -fold forked stripes. As such, there are many methods for detecting optical OAM using interference, like the Young's double-slit interference [73], [74], the multipoint interference [75], and the annular aperture interference [76]. However, with these



TABLE V: Comparison of Optical OAM Detection Methods.

Features	Holographic gratings	Dove prism interferometers	Mode converters
Cost	Low	Low	Low
Conversion efficiency	Low, no higher than $1/N$	High, near 100%	Relatively high
OAM mode	Composite mode detection; The number is limited by the size of the grating	Composite mode sort; The more the number, the more complicated the device	Composite mode sort; Adjacent OAM state cannot be effectively separated
System complexity	Low	High	Low

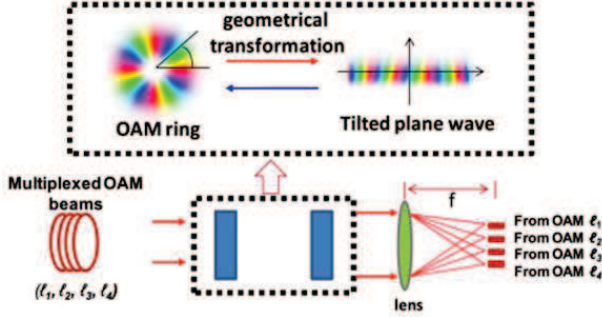


Fig. 14: Principle of the OAM mode converter based on geometrical transformation.

methods it is difficult to correctly detect the intended OAM mode because of the complexity of the received interference pattern. A simpler method is to use a Mach-Zehnder interferometer with a Dove prism placed in each arm to detect single photon OAM [65], called *Dove prism interferometer*, as shown in Fig. 12. The angle of rotation between the two Dove prisms is  $\alpha/2$ , and the rotation angle of the passing beam is  $\alpha$ . Correspondingly, the phase difference between the two arms is  $\ell\alpha$ . If  $\alpha/2 = \pi/2$ , by correctly adjusting the path length of the interferometer, all beams with even  $\ell$  have constructive interference at one output port and cancellation at the other output port, while for all beams with odd  $\ell$  it is just the opposite. Therefore, such an interferometer can achieve OAM mode odd- $\ell$  and even- $\ell$  separation at the single photon level. As shown in [77], the improved interferometer system is capable of detecting a single photon OAM and SAM. By cascading multiple interferometers as shown in Fig. 13, it is possible to generalize this architecture to detect any number of OAM modes, and the theoretical efficiency is close to 100%. In principle, detecting  $N$  OAM states requires  $N - 1$  interferometers. Therefore, such an interferometer device is too complex for practical applications with a large number of OAM modes.

After passing through a lens, a plane wave converges into a point, whose lateral position on the focal plane depends on the lateral phase gradient of the plane wave. Note that the two plane waves need at least a phase difference of  $2\pi$  to make the distance between the two focal points larger than the Rayleigh resolution limit. Using this idea, [78] proposes a mode conversion method for sorting OAM modes. The *mode converter* consists of a converter and a corrector. The converter

implements the conversion from a Cartesian coordinate system to a log-polar coordinate system, so that a point  $(x, y)$  on the input plane is converted into a point  $(u, v)$  on the output plane, where the conversion law is  $u = -a \ln(\sqrt{x^2 + y^2}/b)$  and  $v = a \arctan(y/x)$ . The corrector is used to compensate the phase distortion caused by the optical path length during the coordinate transformation. Thus, an annular beam with a spiral wavefront on the input plane is mapped to a rectangular beam with a tilted wavefront on the output plane. The rectangular beams with different lateral phase gradients are focused by the lens on different lateral positions on the focal plane, effectively separating the different OAM modes. In [79] an OAM mode converter composed of two custom refractive optical elements is designed to achieve higher conversion efficiency. Nevertheless, there is a limit to the mode converters due to the overlap between the focal points of two adjacent OAM modes. In [80] it is shown that by using a series of unitary optical transformations, which generate multiple copies of the rectangular beams, it is possible to achieve a larger separation between OAM modes, trading larger efficiency with higher system complexity.

In addition to the above methods, there are other techniques for separating OAM modes. In [81] it is proposed a method based on the use of  $q$ -plates. The radius ratio method can be used to detect certain special optical OAM [82], [83]. Photonic integrated circuits are well compatible with single-mode fibers while achieving optical OAM multiplexing and demultiplexing [84], [85].

Three common methods for detecting optical OAM are compared in Table V.

### B. Radio OAM

As in optics, the detection of OAM at radio frequencies can be achieved by employing carefully designed *inverse SPPs*. It is also possible to detect the radio OAM mode by observing the interference pattern of a vortex wave and a plane wave. Nevertheless, many detection methods in optics are no longer applicable at radio frequencies and some new methods have been proposed.

In [31] *interference phase detection* is used to separate two electromagnetic beams with topological charges of  $\ell = 0$  and  $\ell = 1$ . In the experiment set-up, two Yagi antennas A and B are connected by a  $180^\circ$  phase-shift cable to form a phase interferometer, designed to reduce background interference in a real environment. As shown in Fig. 15, if the device is fully

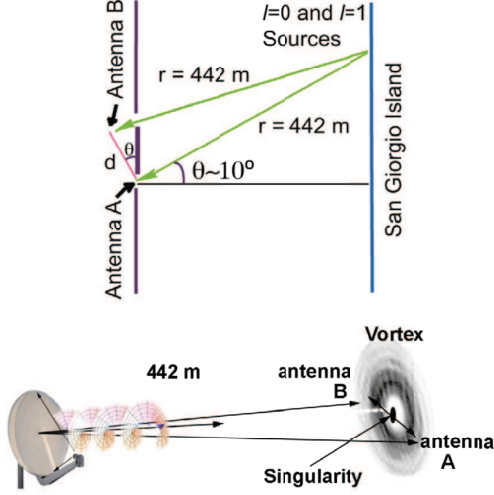


Fig. 15: Sketch of the famous Venice experiment of radio OAM communications [31].

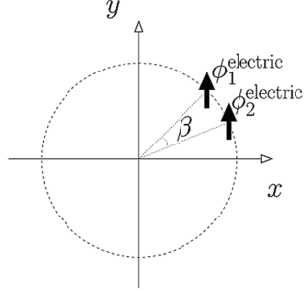


Fig. 16: The illustration of the phase gradient method [86].

aligned, the vortex electromagnetic beam with  $\ell = 1$  will produce a phase difference of  $180^\circ$  between receive antennas  $A$  and  $B$ . This phase difference is compensated by the cable line phase delay, so that the received interference intensity is maximized. For a beam with  $\ell = 0$ , there is only the phase delay of the cable, and the intensity is minimal. In this way, it is possible to separate beams with different wavefront characteristics. When the interference phase detection method is used for more radio OAM modes, the receiving device becomes very complicated.

In 2010, Mohammadi et al. proposed two methods to estimate far-field OAM modes in radio beams, the *single-point estimation method* and the *phase gradient method* [86]. The single-point estimation method uses an approximation for OAM in the far-field to estimate the OAM from the measurements at a single point of the vertical and the transverse components of the electric field. This method is efficient for the detection of OAM with low mode numbers. Compared with the single-point estimation method, the phase gradient method is more intuitive and effective. As shown in Fig. 16, the measurement set-up consists of two test points separated by an angle  $\beta$  on a circumference at the receiving end. If the measured phases are  $\phi_1$  and  $\phi_2$ , respectively, the OAM mode will be  $\ell = (\phi_1 - \phi_2)/\beta$ . In order to accurately detect the

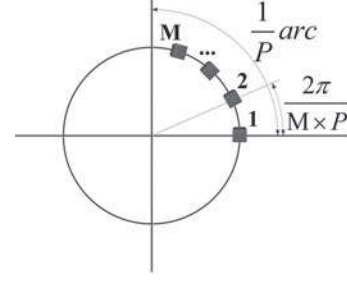


Fig. 17: Schematic of the PASR scheme [87].

OAM mode, the angle  $\beta$  between the two test points should satisfy the relationship  $\beta < \pi/|\ell|$ . The phase gradient method requires that the center of the receiving circle is aligned with the center axis of the vortex beam, otherwise there will be large errors. Generally, it can only be used to detect single-mode OAM beams, but with some modifications, it can also achieve accurate measurement of two mixed modes [88].

UCAAs are used not only for radio OAM generation but also for OAM detection [89]. The condition for detection is that the two arrays are aligned, i.e, the cross section of the receiving circular array  $C$  should be perpendicular to the beam axis and its center should coincide with the axis. UCAAs can demultiplex several radio OAM modes. The whole process of OAM demultiplexing can be seen as some sort of spectral analysis of the received vortex electromagnetic waves. When the mode number  $\ell'$  of the circular array  $C$  is different from one of the beam modes  $\ell$ , the result of the spectral analysis tends to 0, conversely, it tends to 1. By selecting different  $\ell'$  values, different information can be extracted from the OAM multiplexed beam. Nevertheless, only one specific OAM mode can be detected at a time and the detection process needs to receive information of the entire wavefront. Due to the divergence of OAM beams, a large receiving array is required to capture the effective power of the OAM beam in the far-field, but this might be difficult to achieve. An answer to the problem of OAM detection in the far-field is *partial aperture sampling receiving* (PASR) [87], which uses partial wavefront information to detect and distinguish different radio OAM modes, as shown in Fig. 17. The PASR, which is a combination of the partial angular receiving aperture method for OAM demultiplexing in optic [90] and a sampling receiving scheme, has a receiving arc which is  $1/P$  of a circumference and employs  $M$  antennas evenly distributed on the arc as signal sampling points. The angle between adjacent antennas is  $2\pi/MP$ . To ensure strict orthogonality and realize non-crosstalk separation of the two OAM modes  $n_1$  and  $n_2$ , they must satisfy simultaneously the two conditions:  $\text{mod}(|\ell_{n_1} - \ell_{n_2}|, P) = 0$  and  $\text{mod}(|\ell_{n_1} - \ell_{n_2}|, MP) \neq 0$ . Although the PASR has certain limitations, it can greatly simplify the scale of the receiving end and is robust to non-ideal OAM beams.

Table VI compares the common detection methods for radio OAM.

TABLE VI: Comparison of Radio OAM Detection Methods.

Features	Interference phase detection	Single-point estimation method	Phase gradient method	UCAAs	PASR
Cost	Low	Low	Low	High	High
Sampling range	Two points	Entire wavefront	Two points	Entire wavefront	Partial wavefront
OAM mode	Composite mode; The higher the number, the more complicated the device	Single mode; It is more suitable for low mode	Single mode	Composite mode; but only one can be detected at a time	Multiple modes; There is a restriction on the use of OAM mode
System complexity	High	Low	Low	High	High

TABLE VII: Summary of OAM Detection Methods.

Methods	Introduction and Features	Remarks
Holographic gratings	A holographic grating with $\exp(-i\ell\theta)$ phase factor can convert vortex beams into plane beams, and a Daman grating can realize parallel detection of multiple OAM modes. Simple and fast; low conversion efficiency, no higher than $1/N$ , where $N$ is the total number of detected modes.	Optical OAM
Dove prism interferometers	By adjusting the rotation angle of the Dove prism, the odd-even sort of OAM modes can be achieved on a single photon level. High conversion efficiency, close to 100%; Any number of OAM modes can be detected by cascading multiple interferometers, while increasing the complexity of the device.	Optical OAM
Mode converters	The geometric transformation is used to map the Cartesian coordinate to the log-polar coordinate, and annular beams with spiral wavefronts are mapped to rectangular beams with tilted wavefronts, which are focused by lens in different lateral positions. High conversion efficiency; adjacent OAM mode cannot be effectively separated.	Optical OAM
Interferometric phase detection	The phase shift cable is used to compensate the phase difference between the receiving antennas, so that the specific OAM mode has the highest intensity and the other modes have the lowest intensity. Intuitive; the receiving device is very complicated when detecting multi-modal OAM.	Radio OAM
Single-point estimation method	It uses an approximation for OAM in the far-field to estimate the OAM from the measurements at a single point of the vertical and the transverse components of the electric field. It is efficient for the detection of OAM with low mode numbers.	Radio OAM
Phase gradient method	Estimate the OAM mode by measuring the phase of two test points separated by an angle $\beta$ , $\ell = (\phi_1 - \phi_2)/\beta$ . Low complexity; small scale; the angle $\beta$ between the test points should satisfy $\beta < \pi/( \ell )$ .	Radio OAM
UCAAs	A receiving circular array C with $\ell = \ell'$ can extract the information carried by the beam with $\ell = \ell'$ from the multiplexed OAM beam. Only one specific OAM state can be detected at a time, and the detection process needs to receive information of the entire wavefront.	Radio OAM
PASR	Demultiplexing is implemented by utilizing partial wavefront information and the orthogonality between OAM modes. Small scale; two multiplexed OAM modes $\ell_{n0}$ and $\ell_{n1}$ must satisfy $\text{mod}( \ell_{n1} - \ell_{n2} , P) = 0$ and $\text{mod}( \ell_{n1} - \ell_{n2} , MP) \neq 0$ .	Radio OAM
Metamaterials	$M$ metamaterials with $\ell = -1$ can convert the component with the mode number $\ell = m$ into a plane wave. Realtime; high conversion efficiency; low flexibility; specific working frequency; it is not suitable for detection of high-mode OAM.	Acoustic OAM

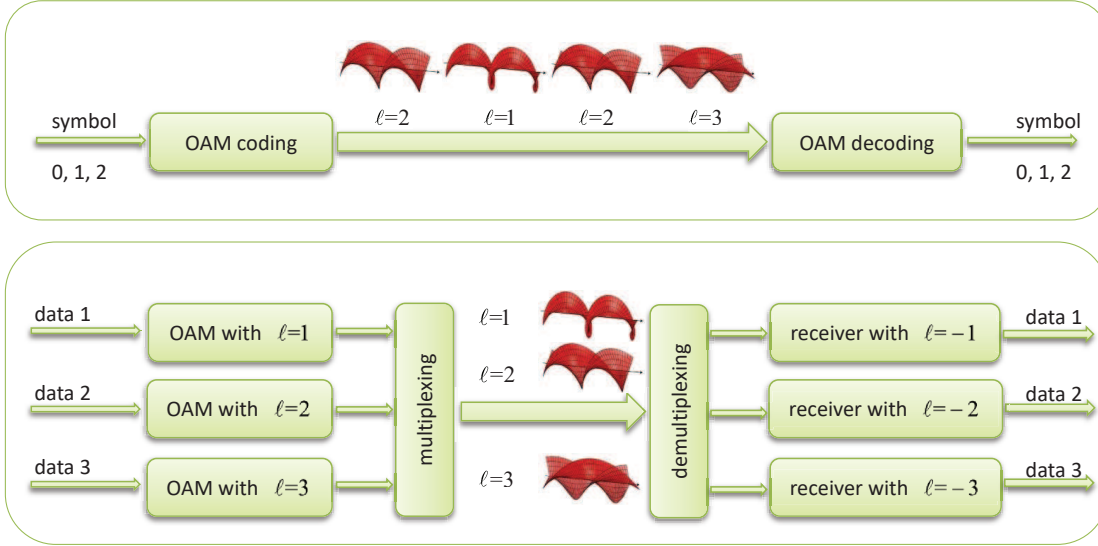


Fig. 18: Schematic diagram of OAM-SK and OAM-DM communications.

### C. Acoustic OAM

As mentioned above, research on OAM detection at acoustic frequencies is still in an early stage. Due to the orthogonality between the OAM eigenstates, Shi et al. use the inner product operation to separate the multiplexed OAM modes received by a transducer array [91]. Recently, Jiang et al. used passive metamaterials to detect acoustic OAM [92]. The structure of such passive acoustic metamaterials has been described in Section II. After that an acoustic beam is passed through a metamaterial with a topological charge of  $\ell = -1$ , the mode number of all multiplexed OAM modes will be reduced by 1. Therefore,  $m$  metamaterials with  $\ell = -1$  can convert the component with the mode number  $\ell = m$  into a plane wave and a non-zero value can be detected at the dark core point of the OAM beam. This non-zero value contains the information carried by the OAM with  $\ell = m$ . This method can realize real-time demodulation of OAM beams and has high conversion efficiency but low flexibility and is not suitable for detection of high-mode OAM.

### D. Summary

Table VII summarizes the common detection methods for OAM. Inverse SPP is a common method for detecting optical OAM and radio OAM. In optical communications, holographic gratings loaded on SLM are commonly used to detect OAM modes. Vortex electromagnetic waves carrying OAM at radio frequencies are generally generated and radiated by using a UCAA and are sampled and received by an antenna array at the receiving end. The sampling point can be a circular array or a partial array or even just two points, as in the case of the phase gradient method. In any case, the reduction of sampling points tends to worsen the receiver performance.

## IV. APPLICATIONS OF OAM IN COMMUNICATIONS

OAM can be employed to transfer information. As shown in Fig. 18, the two main transmission technologies are *OAM*

*shift keying* (OAM-SK), where the information is encoded in the value  $\ell$  of the OAM beam, and *OAM division multiplexing* (OAM-DM), where the information is multiplexed in multimodal OAM beams. OAM-DM uses the vortex beam as the carrier of information modulation so that the data is loaded onto different OAM modes and then multiplexed and transmitted. Because the OAM with different integer  $\ell$  values are mutually orthogonal, vortex beams carrying different OAM provide independent communication channels for efficient information transmission. Compared with OAM-SK, OAM-DM system has higher spectral efficiency and exhibits lower bit error rates.

OAM-DM is a subset of space-division multiplexing (SDM) and can be compatible with different modulation formats, such as  $M$ -ary amplitude-shift keying ( $M$ -ASK),  $M$ -ary phase-shift keying ( $M$ -PSK) and  $M$ -ary quadrature amplitude modulation ( $M$ -QAM), as well as other multiplexing techniques such as frequency-division/wavelength-division multiplexing (FDM/WDM) and polarization-division multiplexing (PDM), thereby further improving the communication system capacity from another dimension. In the OAM-DM system,  $N$  OAM waves carrying information are multiplexed, and the obtained field can be expressed as

$$U_{MUX}(r, \theta, t) = \sum_{p=1}^N S_p(t) A_p(r) e^{i\ell_p \theta}, \quad (1)$$

where  $S_p(t)$  is the modulated data signal on the  $p$ th OAM mode and  $A_p(r)$  is the complex electric field amplitude of the  $p$ th OAM mode. Then, at the receiving end, the multiplexed OAM wave is multiplied by an anti-helical phase factor  $\exp(-i\ell_q \theta)$ , which is achieved by using an inverse SPP or an antenna array. The OAM wave with  $\ell = \ell_q$  is converted into a plane wave and can be easily separated from other vortex waves with  $\ell = \ell_p - \ell_q$ , thus achieving demultiplexing. Eventually, the data information carried by the OAM wave with  $\ell = \ell_q$  can be obtained.



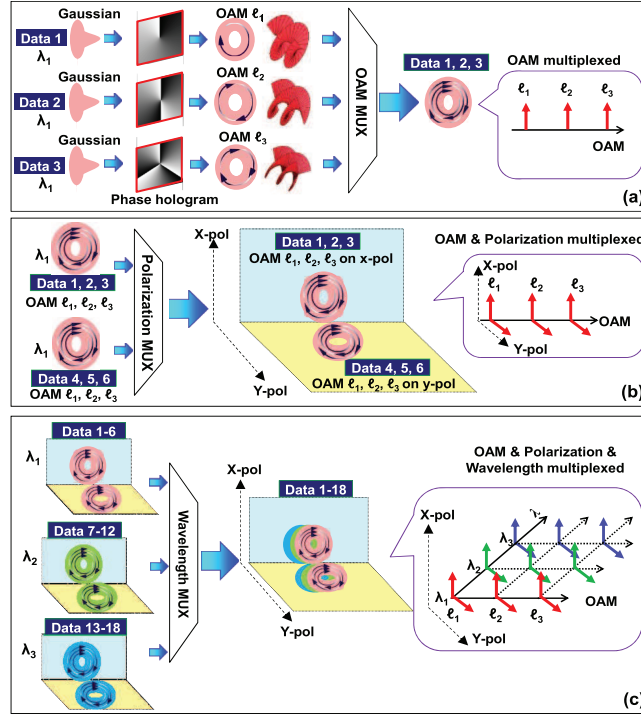


Fig. 19: Concept of using three-dimensional multiplexing to increase the multiplexed data channels. (a), (b), and (c) are performed successively to achieve OAM-DM, PDM, and WDM, respectively [93].

#### A. Free-Space Optical OAM Communications

In 2004, Gibson et al. [67] demonstrated for the first time that OAM-SK modulation can be used for free-space optical (FSO) communications with good results. The transmitter maps the information data on the OAM beams' topological charge, which belongs to the set  $\mathcal{L} = \{-16, -12, -8, -4, +4, +8, +12, +16\}$ . At the receiving end, two vertically stacked forked gratings are used to detect the transmitted OAM modes. To compensate for small perturbations in alignment, a Gaussian beam with  $\ell = 0$  is used as a reference signal. In [94] 16 superimposed OAM modes are employed to transmit information over a 3 km intra-city link. At the receiver the beam topological charge was recovered by a non-coherent detection scheme aided by an artificial neural network. This experimental scheme has recently been extended to a 143 km free-space link between the two Canary Islands of La Palma and Tenerife [95].

If an OAM-SK system with  $L$  different topological charges can transmit up to  $\log_2(L)$  bits per beam, an OAM-DM system that multiplexes  $L$  modes can transmit up to  $L$  bits per beam. For example, consider the case with  $\mathcal{L} = \{\ell_0, \ell_1\}$ , i.e.,  $L = 2$ . With OAM-SK it is possible to transmit one bit per beam (0 if  $\ell = \ell_0$  and 1 if  $\ell = \ell_1$ ). With OAM-DM, the on and off states of each OAM mode can represent either a "1" or a "0", so that the two-bit set of  $\{00, 01, 10, 11\}$  can be mapped on the multiplexed modes  $\{00, 0\ell_1, \ell_0 0, \ell_0 \ell_1\}$ . Using this idea, [96] transmits the information in free space by multiplexing four OAM modes employing a phase hologram loaded on a SLM. Subsequently, this method was used to implement the encoding of two-dimensional images [71], [97].

In order to meet the ever-increasing demands for higher data rates, OAM multiplexing can be combined with different modulation formats and different multiplexing techniques to achieve high-speed communication in multiple dimension. A data link multiplexing the signal in three dimensions is shown in Fig. 19. Three OAM beams with  $\mathcal{L} = \{\ell_1, \ell_2, \ell_3\}$ , carrying the modulation information data 1, data 2 and data 3, are multiplexed into one multimodal beam. A second OAM beam with the same set of modes  $\mathcal{L}$  carrying the data streams data 4, data 5 and data 6 is multiplexed with the first one employing orthogonal polarizations. Finally, three polarization-and-OAM-multiplexed beams carrying three different sets of information streams, data 1-6, data 7-12 and data 13-18, are transmitted at three different wavelengths  $\lambda_1, \lambda_2$  and  $\lambda_3$ . In a recent laboratory experiment [98], a transmission rate of 2.56 Tbps and a spectral efficiency of 95.7 bps/Hz have been achieved by using  $20 \times 4$  Gbps 16QAM signals on 8 OAM modes, 2 polarization states, and two sets of concentric rings. In [99] a transmission rate of 100.8 Tbps is achieved by transmitting 100 Gbps QPSK signals on 12 OAM modes, 2 polarization states, and 42 wavelengths. In a similar fashion, in [100] a transmission rate of 1.036 Pbps with a spectral efficiency of 112.6 bps/Hz has been achieved by multiplexing 54.139 Gbps OFDM-8QAM signals over 368 WDM wavelengths, 2 polarization states and 26 OAM modes. In addition to these lab-scale high-rate data experiments, a 400 Gbps transmission rate has been achieved over an outdoor link of about 120m by using 100 Gbps QPSK signals on 4 OAM modes [93].

It is well known that Laguerre-Gaussian (LG) beams are identified by two parameters: the azimuthal index  $\ell$  and the

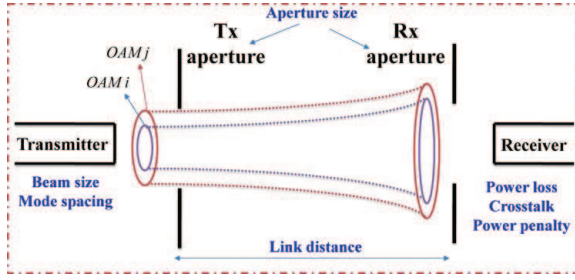


Fig. 20: OAM beam divergence in FSO communications [106].

radial index  $p$ . The former is the topological charge, which characterizes the beam OAM, the latter is related to the number of radial nodes on the cross section of the beam intensity, typically assuming a non-zero integer value. Most of the literature on OAM beams is devoted to LG beams with an azimuthal index  $\ell > 0$  and a radial index  $p = 0$ . Because the radial index  $p$  can be used as a radial degree of freedom, just as  $\ell$  can provide an azimuthal degree of freedom, recently, a LG beam with  $p > 0$  has received some attention [101], [102]. Indeed, LG beams with different  $p$  and  $\ell$  form a complete set of orthogonal mode bases. By multiplexing LG beams with different  $p$ , the system capacity and transmission rate can be improved. In addition to LG beams, Bessel beams with non-diffractive properties can also carry OAM. Because of their self-healing properties for obstacles they have a great application potential in FSO communications [103], [104]. Perfect vortex beams, obtained by Fourier transformation of BG beams, have the attractive property that the radius is independent of the OAM mode [105].

OAM beams have some inherent characteristics that limit their application in FSO communication systems, such as *beam divergence* and *misalignment*. The OAM beam radius increases with the propagation distance, and different modes have different degrees of divergence, as shown in Fig. 20. When a finite size receiving aperture is used, the divergence of the beam can cause system power loss. This misalignment between transmitter and receiver includes lateral displacement and receiver angle errors [106], as shown in Fig. 21. In general, to avoid not only energy loss but also serious crosstalk between channels, FSO links using OAM require strict alignment and phase matching.

For OAM FSO links, *atmospheric turbulence* is the most important impairment, since changes of the atmosphere refractive index due to temperature and pressure non-uniformities can destroy the helical wavefront of vortex beams, causing both receiving energy fluctuations and crosstalk between OAM channels, as shown in Fig. 22. Paterson [108] and Tyler [109] used the Kolmogorov spectral statistical model to quantitatively analyze the effects of atmospheric turbulence on OAM beams. This theoretic model has been later verified in [107], [110] by simulating turbulence in a laboratory. Empirical and theoretic results show that as the turbulence intensity increases, the power of a transmitted OAM mode begins to leak into its adjacent modes, ending to be evenly distributed in the case of strong turbulence. To improve the performance of OAM FSO

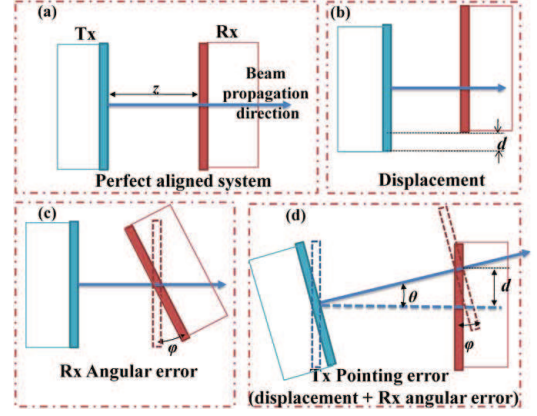


Fig. 21: Alignment between the transmitter and the receiver for (a) a perfectly aligned system, (b) a system with lateral displacement, (c) a system with a receiver angular error, and (d) a system with a transmitter pointing error [106].

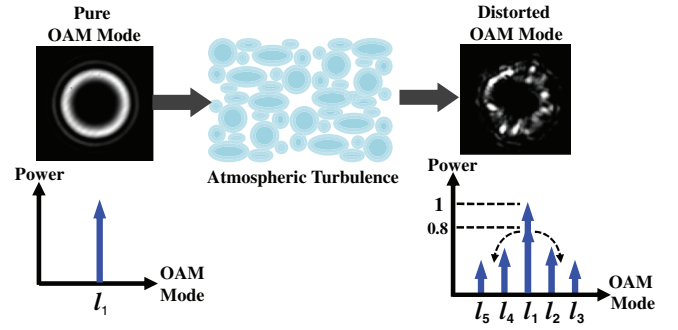


Fig. 22: Concept diagram of the effects of atmospheric turbulence on an OAM beam. A distorted OAM mode can be decomposed into multiple OAM modes [107].

communications, some techniques for mitigating the effects of turbulence have been proposed and they can be categorised as *adaptive optics (AO) compensation*, if they compensate the impairments in the optical domain, or *signal processing-based mitigations*, if they operate in the electrical domain [111].

### B. Optical OAM Fiber Communications

As mentioned above, OAM FSO communication links are greatly affected by beam divergence and atmospheric turbulence. In recent years, research has focused on OAM-based optical fiber communications, which do not need to take these effects into account. Conventional optical fiber communications utilize SDM by using multicore fibers (MCF) [112], [113] and few-mode fibers (FMF) [114] to increase system capacity and spectral efficiency. Multicore fibers require complex manufacturing, while multimode fibers rely on digital signal processing (DSP) algorithms based either on adaptive optics feedback or complex multiple-input multiple-output (MIMO) methodologies to solve the problem of mode coupling caused by random perturbations in fibers or incomplete mode-conversion. OAM technologies have the potential to increase the system throughput of optical fiber communication

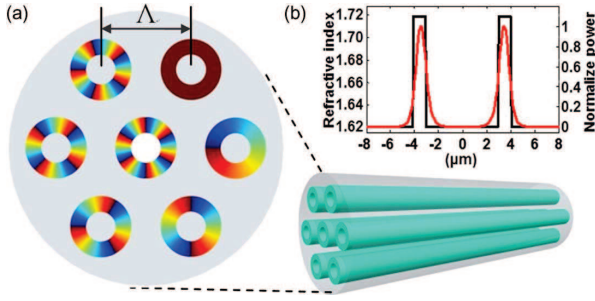


Fig. 23: (a) 3D structure and cross-section of multi-OAM-mode multi-ring fiber (MOMRF). (b) Index profile of single ring (black) and mode profile of  $TE_{01}$  mode (red) in the ring [119].

systems with low complexity DSP algorithms or even without any DSP algorithm.

Bozinovic et al. first demonstrated the feasibility of transmitting OAM modes in 20 m and 900 m long fibers [115], [116]. In a later experiment, a transmission rate of 400 Gbps was achieved using four OAM modes at a single wavelength and a transmission rate of 1.6 Tbps was achieved using two OAM modes over 10 wavelengths [117], employing a specially designed circularly symmetric fiber over 1.1 km long. These experiments have shown that OAM can provide an additional degree of freedom for data multiplexing in fiber networks. At present, research on OAM-based optical fiber communications mainly focuses on fiber design that supports stable transmission of multiple OAM modes. In 2012, Birnbaum et al. designed a 0.05 up-doping ring fiber to support up to 10 OAM modes, while maintaining radial single-mode conditions [118]. In 2013, Li et al. designed a multi-OAM-mode multi-ring fiber (MOMRF) that supports multimode OAM transmissions [119]. As shown in Fig. 23, the fiber consists of seven rings, each supporting 18 OAM modes. Mode crosstalk and inter-ring crosstalk are reduced by increasing the effective refractive index and the distance between rings. In addition, this technology is compatible with WDM and advanced multilevel amplitude/phase modulation formats, which makes it possible to realize a total transmission capacity in the range of the petabits-per-second and hundredbits-per-second-per-hertz aggregate spectral efficiency. Some new types of microstructure fibers have also been proposed for multi-OAM transmissions [120], [121].

Recently, some studies have explored the potentials of the conversion between linear polarization (LP) modes and OAM modes in FMF-based mode-division multiplexing (MDM) systems. In [122], Zeng et al. designed a novel all-fiber OAM generator, which is cascaded by a mode-selective coupler and a few mode-polarization maintaining fiber, to convert  $LP_{01}$  mode to OAM mode. In [123] a series of  $LP_{11}$  modes with micro-phase difference distribution are generated by twisting a few-mode fiber long period grating (FMF-LPG), these  $LP_{11}$  modes are then superimposed on the fiber to generate OAM modes. In [124] Li et al. proposed and demonstrated a controllable wideband fiber OAM converter. As shown in Fig.

24, the converter consists of a two-mode fiber (TMF) with specific offsets and tilt angles, two polarization controllers (PCs) and a polarizer. The input end of TMF is attached to a standard single-mode fiber. By adjusting the two PCs, an input fundamental mode can be selectively converted to high order  $LP_{11}$  modes or OAM modes with  $\ell = \pm 1$ .

OAM multiplexing provides an effective solution for improving the capacity and the spectral efficiency of optical fiber communications. Unfortunately, conventional fiber (SMF ITU-T G.652) is single mode fiber at 1550 nm and does not support OAM modes. However, the number of OAM modes supported increases as the wavelength decreases. While it is feasible to transmit multiple OAM modes in the conventional G.652 fiber, the problem of how to guide these OAM modes needs to be considered. In [125] the OAM mode properties at the three RGB wavelengths (red at 632.8nm, green at 532nm and blue at 476.5nm) are theoretically analyzed. The number of guided circular OAM modes, synthesized by a proper linear combination of degenerate fiber eigenmodes, supported by conventional G.652 fiber in the RGB wavelengths is 12, 20 and 24, respectively. The results clearly show that G.652 fiber can support red, green and blue modes, at least for short distance communications.

At present, OAM-based optical fiber communication technology is an active field of continuous research, since there are still many open problems about mode generation, mode coupling, optical fiber transmission, demodulation and optical fiber devices.

### C. Radio OAM Communications

The application of OAM to radio communications is expected to be a possible solution to the problem of spectrum scarcity and it has, accordingly, received widespread attention. The first OAM-based wireless communication experiment that successfully separated two radio signals at the same frequency was presented in [31]. A Yagi antenna and a spiral parabolic antenna were used to transmit a plane electromagnetic wave and a vortex electromagnetic wave, respectively, at a distance of 442 meters. Subsequently, a 4 Gbps uncompressed video transmission link over a 60 GHz OAM radio channel has been implemented [126]. In the RF or millimeter wave bands, provided that there is a line-of-sight (LOS) link so to guarantee the correct transmitter-receiver alignment, OAM can be used to encode information [127], and can also be multiplexed and combined with other technologies [128]–[130]. In [128] are reported the results of an experiment in the 28 GHz band that has achieved a 32 Gbit/s capacity and about 16 bit/s/Hz spectral efficiency by combining 4 OAM modes carrying 4 Gbit/s 16QAM modulated signals with 2 polarization states. Some specially designed structures can generate multiple radio OAM beams at the same time, or even directly generate multiplexing beams, which can carry independent data streams in the same medium, such as dual OAM mode antennas based on ring resonators [131] and thin metamaterial plates based on rectangular apertures [132].

It is well known that multiple-input multiple-output (MIMO) is a key technology that can greatly increase the



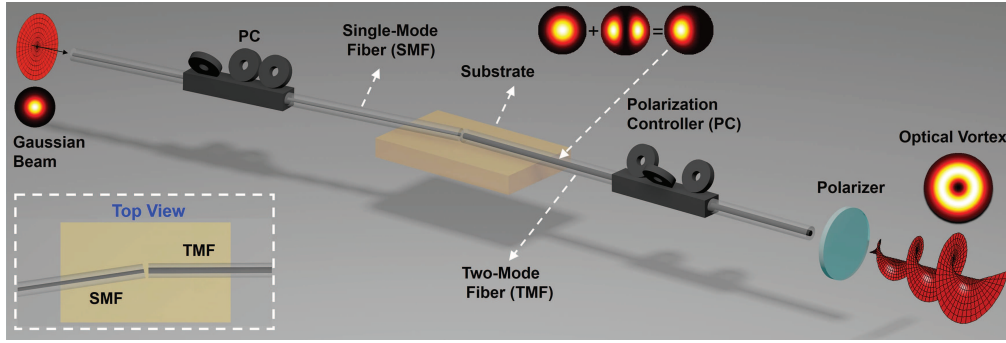


Fig. 24: Concept of controllable broadband fiber-based OAM converter [124].

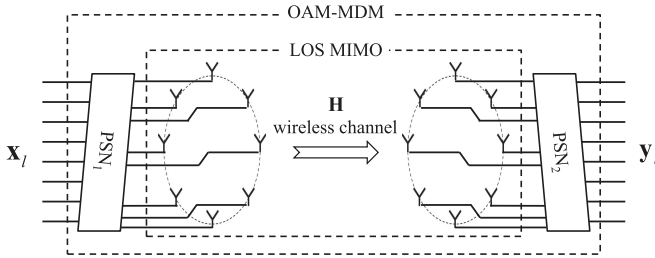


Fig. 25: System models for the UCA-based OAM-MDM and LOS MIMO communications [133].

capacity of wireless communication systems by using multiple transmitting and receiving antennas. The relationship between MIMO SDM and OAM multiplexing has caused a heated debate in the academia. It has been pointed out that radio OAM systems based on uniform circular array (UCA) are a subset of MIMO systems and do not really provide additional capacity gain [134], [135]. But in practice there are differences between the two approaches. For example, in a keyhole channel traditional MIMO systems have very poor performance, while UCA-based OAM benefits of the fact that the keyhole does not change the helical phase structure of OAM [136]. In terms of capacity over a LOS link, a UCA-based OAM system is equivalent to a traditional MIMO system from the perspective of channel spatial multiplexing [137]. However, OAM receivers have a lower complexity because, unlike traditional MIMO systems, the inherent orthogonality between OAM states can mitigate inter-channel interference [133]. A sketch of a system employing OAM-MDM and LOS MIMO communications is shown in Fig. 25, where a phase-shifted network is used to multiplex and demultiplex OAM modes with a reduced computational load at the receiving end of the OAM system. Moreover, as described in Section II, radio OAM is produced not only by employing antenna arrays, but also by using SPP or spiral parabolic antennas or other single transmit antennas. Combining OAM with traditional MIMO technology can result in higher capacity gains [138], [139] or provide a more flexible system design [140], [141]. A  $2 \times 2$  antenna aperture architecture, where each aperture multiplexes two OAM modes, is implemented in the 28 GHz band to achieve a 16 Gbit/s transmission rate. At the receiving end, MIMO signal processing is employed to mitigate inter-channel

interference [141]. Such a system architecture incorporating OAM multiplexing and MIMO technology can also be used for FSO communication links [142].

As it happens for optical OAM, radio OAM is affected by beam divergence and misalignment between the transmitter and the receiver. The fact that the wavelengths at radio frequencies are much larger than the wavelengths of light makes the problem of divergence significantly more important, greatly limiting the achievable distance of OAM links. Both wireless communication and FSO communication require perfect alignment of the transmitter and the receiver. A UCA-based beam steering method for wireless communication systems using OAM can circumvent the large performance degradation in the misalignment cases [143]. On the other hand, larger wavelengths reduce the impact of atmospheric turbulence, which is not a primary impairment for wireless communication links. However, in wireless communication systems, multipath effects caused by beam spreading and reflections of surrounding objects also affect the system performance. The multipath effects caused by specular reflection from a plane parallel to the propagation path in OAM-based wireless communications have been discussed in [144], [145]. An OAM channel with larger  $\ell$  has stronger intra- and inter-channel interference due to OAM beam divergence. Recently, in order to mitigate multipath effects, a transceiver architecture for broadband OAM orthogonal frequency-division multiplexing (OFDM) wireless communication systems has been proposed, which uses a baseband digital 2-D Fast Fourier Transform (FFT) algorithm to generate and receive the OAM-OFDM signal, thereby reducing energy consumption and hardware cost [146].

#### D. Acoustic OAM Communications

In the field of acoustics, OAM-based communication technology is still in its infancy. In 2017, Shi et al. [91] used eight acoustic OAM modes to transmit the letters of the word 'Berkly', in ASCII binary protocol, achieving a high spectral efficiency of  $8.0 \pm 0.4$  bit/s/Hz. In details, each OAM mode carries 1-bit information in 1-byte binary symbols of the letters, as shown in Fig. 26 (A). These eight OAM orthogonal bases are multiplexed and transmitted by a single transducer array. At the receiver, another transducer array receives the signal and then demultiplexes it, exploiting the orthogonality



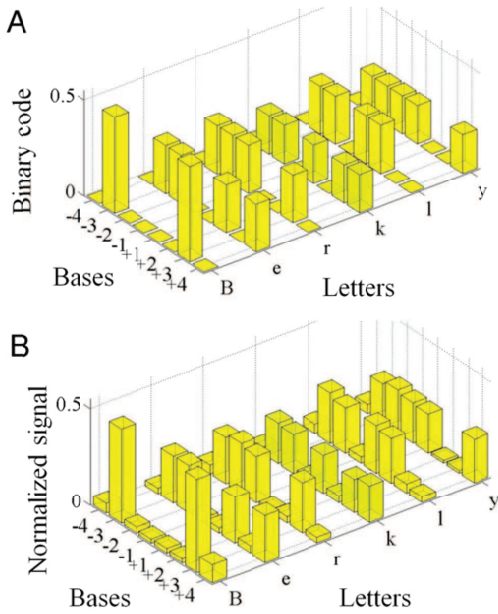


Fig. 26: (A) Encoding of the letters of the word ‘Berkly’ and (B) decoding after transmission with 8 OAM modes [91].

between OAM modes. The recovered signal is shown in Fig. 26 (B). Instead of using OAM modes to encode data, Jiang et al. directly loaded the data onto the acoustic OAM channels and established a real-time information transmission system based on passive metamaterials [92]. These studies have shown that in acoustic communications OAM can provide an additional dimension to increase the transmission rate and the spectral efficiency.

Because microwaves and mid- and far-infrared radiations have strong intrinsic absorption under water, and light is easy to be scattered by objects in the ocean such as small particles, debris and marine life, sound waves are the only information carrier for underwater long-distance (more than 200 meters) communications. Applying OAM to underwater acoustic communications is expected to increase system capacity and spectrum efficiency, even if this requires further experimental verification.

## V. APPLICATION OF OAM IN PARTICLE MANIPULATION AND IMAGING

### A. Optical and Acoustical Particle Manipulation

OAM has found applications also outside the field of wireless, optical and acoustic communications. Thanks to the work of Nobel laureate Arthur Ashkin, light has since long been used to trap small particles in what we call *optical tweezers*. Optical tweezers use a single tightly-focused beam with a large enough gradient force around the focus to overcome the linear momentum of the light, attracting the particles toward the center [147]. In 1995, [148] has shown that, by transferring the OAM carried by photons to small particles, lasers with OAM can be employed to achieve the rotation of the trapped particles, transforming the tweezers into *optical spanners* that cause the objects to spin [149]. When a circularly polarized

LG beam with  $\ell = 1$  is used to interact with the particles, the total angular momentum is either  $\sim 0.06\hbar$  or  $\sim 2.06\hbar$  per photon depending on the spin direction of the beam, resulting in the stopping or the rotation of the particles. Similarly, using the same method but with a different beam with  $\ell = 3$ , two different rotational velocities of the particles can be observed [150]. In the above work, the size of the particles is larger than the beam, and the particles are considered to be trapped on or near the axis. When the size is smaller than the ring beam, the particles are generally trapped in the off-axis area. In this case, the spin of the trapped particles depends on the SAM of the ring beam, and the ring beam with the helical phase structure associated with OAM imposes an azimuthal scattering force on the particle to rotate the particle around the beam axis [151], [152].

When interacting with the absorbing particles, OAM carried by acoustic vortices can also be transferred to the particles, exerting a torque on them. This mechanical effect can be applied as *acoustic tweezers* and *acoustic spanners*, and has great application prospects in the field of ultrasonic medicine. Courtney et al. implemented acoustic tweezers using first-order and superimposed high-order Bessel acoustic vortices [153], [154]. Their experiment uses a transducer array to generate the required Bessel acoustic vortex field and can control the movement of the vortex center by adjusting the drive signal of the array element, achieving particle capture at different locations. Unlike optical vortices, acoustic vortices cannot carry SAM and, when vortex beams act on particles, only OAM transfer occurs. In [55] it is experimentally demonstrated that acoustic vortices in free space can transmit acoustic OAM to an object and make it rotate. The experiment uses a torsion pendulum to measure the angular momentum of acoustic vortices and compares the effective acoustic torque obtained with different topological charges. In 2012, Anhäuser et al. quantitatively measured the amount of OAM transmitted by an acoustic vortex to an absorbing disk in a viscous liquid [155].

### B. Optical and Radar Imaging

OAM applied to an optical or radar imaging system can break the limits of resolution or sensitivity. The stimulated emission depletion (STED) microscope uses an annular beam with a helical phase distribution to suppress the fluorescence of particles around the scanning point, achieving a resolution beyond the diffraction limit [156]. Applying OAM to diffraction tomography can make a significant breakthrough with respect to the diffraction limits associated with traditional techniques [157].

Inserting a spiral phase mask into the Fourier plane of an optical imaging system can effectively convert the point spread function of the system into an annular intensity cross section with an  $\exp(i\ell\theta)$  phase distribution [158]. This can be used to observe the light around bright objects [159]. In [160] this method is used to suppress the brightness of stars and make orbital planets more visible. OAM can also be combined with optical microscopes: spiral phase masks can be placed on the Fourier plane of a microscope to achieve

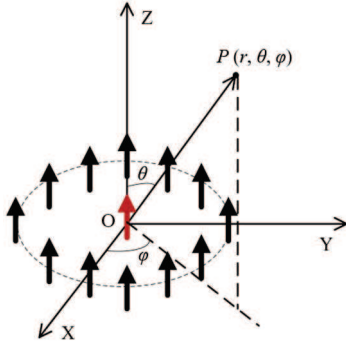


Fig. 27: Schematic diagram of radar target detection based on vortex electromagnetic waves [164].

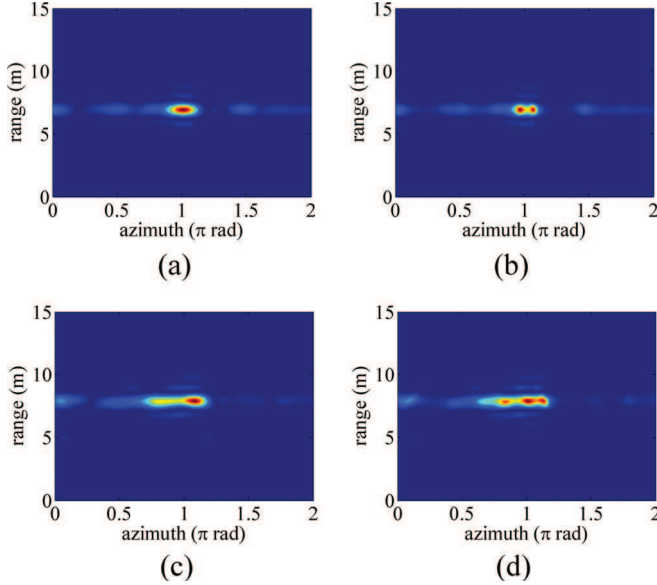


Fig. 28: Comparisons of imaging results between the traditional array imaging and the electromagnetic vortex imaging. (a) Traditional array imaging of two reflectors, (b) electromagnetic vortex imaging of two reflectors, (c) traditional array imaging of three reflectors, and (d) electromagnetic vortex imaging of three reflectors [165].

*spiral phase contrast imaging*, which is often used to observe bright edges of phase objects [161], [162]. In addition, when a spiral phase beam is used as reference wave of an interference system, the interference pattern is a chiral spiral stripe, so that the protrusions and depressions of the sample surface can be distinguished by observing the direction of rotation of the spiral stripe [163].

In 2013, [166] applied OAM to the field of radar imaging, and proposed the idea that vortex electromagnetic waves have the potential for radar target imaging. The paper developed an echo model of the ideal point scattering target under vortex electromagnetic wave illumination and implemented radar imaging using the back projection algorithm and the filtered FFT based algorithm. Afterwards, [164] established echo signal models for multiple input multiple output and multiple input single output systems. The OAM-based radar

imaging system model is shown in Fig. 27. Assume that the target is made up of  $M$  ideal scattering points, denoted by  $P_m(r_m, \theta_m, \varphi_m)$  and corresponding radar cross section (RCS)  $\sigma_m$ ,  $m = 1, \dots, M$ . In the multiple input single output mode, a single antenna is set at the original point to receive the echo signal. the normalized echo signal is expressed as

$$s(k, \ell) = \sum_{m=1}^M \frac{\sigma_m}{r_m^2} e^{i2kr_m} e^{i\ell\varphi_m} J_\ell(ka \sin \theta_m), \quad (2)$$

where  $k = 2\pi f/c$  is the wave number,  $J_\ell(ka \sin \theta)$  is the Bessel function of the first kind, and  $a$  is the radius of UCA. As can be seen from (2), the OAM mode number  $\ell$  and the azimuth  $\varphi$  satisfy the dual relationship, and so do the frequency  $k$  and target range  $r$ . Thus, the 2-D FFT can be used in estimating the range and azimuth of targets. This shows that the OAM-based radar imaging system has the prospect of acquiring the azimuth information of target.

OAM-based radar detection provides a new set of ideas and solutions for the development of accurate target imaging. Due to its spiral phase structure, a vortex electromagnetic wave carrying OAM can be regarded as a traditional plane wave illuminating a target from multiple consecutive angles, which is equivalent to realizing continuous sampling in a two-dimensional space in a short time, obtaining a good degree of spatial diversity. In addition, when vortex electromagnetic waves of different modes with different spiral phase structures hit the target in space there are phase differences, which make the backscattering characteristics different and improve the radar cross-section diversity gain [167]. In conventional radar imaging, the azimuth resolution is generally enhanced by increasing the aperture size, while vortex electromagnetic waves can provide a high resolution, which is not limited by the array aperture. This has been verified by a proof-of-concept experiment [165] as shown in Fig. 28. Applying multimode OAM to radar imaging enables azimuthal imaging without relative motion. Similarly, vortex electromagnetic waves can also be applied to synthetic aperture radar (SAR) imaging to obtain higher azimuthal resolution than planar electromagnetic waves [168].

Recently, research on OAM radar imaging has mainly focused on beam calibration techniques and azimuth imaging algorithms. Because the center of vortex electromagnetic beams is null and the angular direction of the main lobe varies with the OAM modes, it is difficult to simultaneously illuminate the target with vortex electromagnetic beams of different modes, which results in limited echo energy. Moreover, the difference of echo intensity will lead to amplitude modulation of the echo signal, resulting in deterioration of imaging. These effects can be mitigated by carefully designing the radius and the excitation of the UCA to adjust the main lobes of the vortex electromagnetic beams [169]–[171]. Due to the existence of the Rayleigh limit, traditional radar imaging algorithms can only provide limited azimuth resolution. Some studies are devoted to finding more efficient algorithms for super-resolution radar imaging based on OAM, such as UCA-based autoregressive models and power spectral density (PSD) estimation algorithm [170], UCA-based echo models and

multiple signal classification (MUSIC) algorithm [172], [173], estimating signal parameter via rotational invariance (ESPRIT) algorithm [174] and least squares algorithm [171], [175].

## VI. CONCLUSIONS

In recent years, OAM has been extensively studied in many fields of application. In this paper, we provide a comprehensive overview of the generation and detection methods of optical, radio, and acoustic OAM, and their emerging applications in communications, particle manipulation and imaging. Especially in the field of communications, a large number of studies have shown that OAM is able to multiplex a set of orthogonal modes on the same frequency channel so to achieve a high spectral efficiency. However, there are still many challenges on the way to the application of OAM in practice. For example, how to generate and detect high-order and multi-mode OAM beams with a finite-size aperture is challenging. For the free-space link, OAM communications face the problems of OAM beam divergence and misalignment, which result in severe performance degradation, and also atmospheric turbulence is a phenomenon that seriously affect performance. In optical fiber communications, how to design a fiber that can support more OAM modes is another problem that is still open. For radio OAM wireless communication, the effect of multi-path should be considered. Research on acoustic OAM communications still needs further exploration. Whether OAM radar imaging has super-resolution performance is controversial theoretically and so on. In spite of so many challenges, based on the current research progress surveyed in this paper, such as the work of Nobel laureate Arthur Ashkin on optical particle manipulation, we remain optimistic that these challenges will be gradually resolved in the near future and that OAM will help to make breakthroughs in future communications systems.

## REFERENCES

- [1] L. Allen, M. W. Beijersbergen, R. J. Spreeuw, and J. P. Woerdman, "Orbital angular momentum of light and the transformation of laguerre-gaussian laser modes," *Physical Review A Atomic Molecular and Optical Physics*, vol. 45, no. 11, p. 8185, 1992.
- [2] B. Thide, H. Then, J. Sjöholm, K. Palmer, J. Bergman, T. D. Carozzi, Y. N. Istomin, N. H. Ibragimov, and R. Khamitova, "Utilization of photon orbital angular momentum in the low-frequency radio domain," *Phys. Rev. Lett.*, vol. 99, no. 8, p. 087701, 2007.
- [3] E. G. Broadbent and D. W. Moore, "Acoustic destabilization of vortices," *Philos. Trans. Roy. Soc. London*, vol. 290, no. 1372, pp. 353–371, 1979.
- [4] B. T. Hefner and P. L. Marston, "An acoustical helicoidal wave transducer with applications for the alignment of ultrasonic and underwater systems," *The Journal of the Acoustical Society of America*, vol. 106, no. 6, pp. 3313–3316, 1999.
- [5] A. M. Yao and M. J. Padgett, "Orbital angular momentum: origins, behavior and applications," *Advances in Optics and Photonics*, vol. 3, no. 2, pp. 161–204, 2011.
- [6] J. M. Vaughan and D. V. Willetts, "Temporal and interference fringe analysis of tem01\* laser modes," *J Opt Soc Am*, vol. 73, no. 8, pp. 1018–1021, 1983.
- [7] K. Kano, Y. Kozawa, and S. Sato, "Generation of a purely single transverse mode vortex beam from a he-ne laser cavity with a spot-defect mirror," *International Journal of Optics*, vol. 2012, no. 2012, p. 10, 2011.
- [8] M. W. Beijersbergen, L. Allen, H. van der Veen, and J. P. Woerdman, "Astigmatic laser mode converters and transfer of orbital angular momentum," *Opt. Commun.*, vol. 96, no. 1C3, pp. 123–132, 1993.
- [9] M. W. Beijersbergen, R. P. C. Coerwinkel, M. Kristensen, and J. P. Woerdman, "Helical-wavefront laser beams produced with a spiral phaseplate," *Opt. Commun.*, vol. 112, no. 5, pp. 321–327, 1994.
- [10] V. B. Yu, M. V. Vasnetsov, and M. S. Soskin, "Laser beams with screw dislocations in their wavefronts," *Nat. Genet.*, vol. 47, no. 1, pp. 429–431, 1990.
- [11] V. Y. Bazhenov, M. S. Soskin, and M. V. Vasnetsov, "Screw dislocations in light wavefronts," *Optica Acta International Journal of Optics*, vol. 39, no. 5, pp. 985–990, 1992.
- [12] N. R. Heckenberg, R. McDuff, C. P. Smith, and A. G. White, "Generation of optical phase singularities by computer-generated holograms," *Opt. Lett.*, vol. 17, no. 3, p. 221, 1992.
- [13] J. E. Curtis, B. A. Koss, and D. G. Grier, "Dynamic holographic optical tweezers," *Opt. Commun.*, vol. 207, no. 1, pp. 169–175, 2002.
- [14] C. Maurer, A. Jesacher, S. Bernet, and M. Ritsch-Marte, "Tailoring of arbitrary optical vector beams," *New Journal of Physics*, vol. 9, no. 13, p. 78, 2007.
- [15] M. Mirhosseini, C. Chen, B. Rodenburg, M. Malik, and R. W. Boyd, "Rapid generation of light beams carrying orbital angular momentum," *Opt. Express*, vol. 21, no. 25, pp. 30 196–30 203, 2013.
- [16] K. J. Mitchell, S. Turtaev, M. J. Padgett, and D. B. Phillips, "High-speed spatial control of the intensity, phase and polarisation of vector beams using a digital micro-mirror device," *Opt. Express*, vol. 24, no. 25, p. 29269, 2016.
- [17] N. Yu, P. Genevet, M. A. Kats, F. Aieta, J. P. Tetienne, F. Capasso, and Z. Gaburro, "Light propagation with phase discontinuities: generalized laws of reflection and refraction," *Science*, vol. 334, no. 6054, pp. 333–337, 2011.
- [18] P. Genevet, N. Yu, F. Aieta, J. Lin, M. A. Kats, R. Blanchard, M. O. Scully, Z. Gaburro, and F. Capasso, "Ultra-thin plasmonic optical vortex plate based on phase discontinuities," *Appl. Phys. Lett.*, vol. 100, no. 1, p. 169, 2012.
- [19] E. Karimi, S. A. Schulz, I. D. Leon, H. Qassim, J. Upham, and R. W. Boyd, "Generating optical orbital angular momentum at visible wavelengths using a plasmonic metasurface," *Light Science and Applications*, vol. 3, no. 5, p. e167, 2014.
- [20] Z. Zhao, J. Wang, S. Li, and A. E. Willner, "Metamaterials-based broadband generation of orbital angular momentum carrying vector beams," *Opt. Lett.*, vol. 38, no. 6, pp. 932–934, 2013.
- [21] W. Wang, Y. Li, Z. Guo, R. Li, J. Zhang, A. Zhang, and S. Qu, "Ultra-thin optical vortex phase plate based on the metasurface and the angular momentum transformation," *Journal of Optics*, vol. 17, no. 4, 2015.
- [22] L. Marrucci, E. Karimi, S. Slussarenko, B. Piccirillo, E. Santamato, E. Nagali, and F. Sciarrino, "Spin-to-orbital conversion of the angular momentum of light and its classical and quantum applications," *Journal of Optics*, vol. 13, no. 6, p. 064001, 2011.
- [23] E. Brasselet, "Nonlinear spin-orbit interaction of light in liquid crystals," *2011 International Workshop on Nonlinear Photonics*, pp. 1–3, Sept 2011.
- [24] E. Hasman, G. Biener, V. Kleiner, and Z. Bomzon, "Space-variant pancharatanmberry phase optical elements with computer-generated subwavelength gratings," *Opt. Lett.*, vol. 27, no. 13, pp. 1141–3, 2002.
- [25] G. Biener, A. Niv, V. Kleiner, and E. Hasman, "Formation of helical beams by use of pancharatanm-berry phase optical elements," *Opt. Lett.*, vol. 27, no. 21, pp. 1875–7, 2002.
- [26] L. Zhu, X. Wei, J. Wang, Z. Zhang, Z. Li, H. Zhang, S. Li, K. Wang, and J. Liu, "Experimental demonstration of basic functionalities for 0.1-thz orbital angular momentum (OAM) communications," *OFC 2014*, pp. 1–3, March 2014.
- [27] A. Bennis, R. Niemiec, C. Brousseau, K. Mahdjoubi, and O. Emile, "Flat plate for OAM generation in the millimeter band," *2013 7th European Conference on Antennas and Propagation (EuCAP)*, pp. 3203–3207, April 2013.
- [28] L. Cheng, L. Hong, and Z. C. Hao, "Generation of electromagnetic waves with arbitrary orbital angular momentum modes," *Scientific Reports*, vol. 4, p. 4814, 2014.
- [29] F. E. Mahmoudi and S. Walker, "Orbital angular momentum generation in a 60ghz wireless radio channel," *2012 20th Telecommunications Forum (TELFOR)*, pp. 315–318, Nov 2012.
- [30] F. Tamburini, E. Mari, T. Bo, C. Barbieri, and F. Romanato, "Experimental verification of photon angular momentum and vorticity with radio techniques," *Appl. Phys. Lett.*, vol. 99, no. 20, p. 321, 2011.
- [31] F. Tamburini, E. Mari, A. Sponselli, F. Romanato, T. Bo, A. Bianchini, L. Palmieri, and G. Smeda, "Encoding many channels in the same frequency through radio vorticity: first experimental test," *New Journal of Physics*, vol. 14, no. 11, pp. 78 001–78 004, 2012.

- [32] G. A. Turnbull, D. A. Robertson, G. M. Smith, L. Allen, and M. J. Padgett, "The generation of free-space laguerre-gaussian modes at millimetre-wave frequencies by use of a spiral phaseplate," *Opt. Commun.*, vol. 127, no. 4, pp. 183–188, 1996.
- [33] Y. Yan, G. Xie, H. Huang, M. J. Lavery, N. Ahemd, C. Bao, Y. Ren, A. F. Molisch, M. Tur, and M. Padgett, "Demonstration of 8-mode 32-gbit/s millimeter-wave free-space communication link using 4 orbital-angular-momentum modes on 2 polarizations," *2014 IEEE International Conference on Communications (ICC)*, pp. 4850–4855, June 2014.
- [34] S. M. Mohammadi, L. K. S. Daldorff, J. E. S. Bergman, R. L. Karlsson, T. Bo, K. Forozesh, T. D. Carozzi, and B. Isham, "Orbital angular momentum in radio system study," *IEEE Trans. Antennas Propag.*, vol. 58, no. 2, pp. 565–572, Feb 2010.
- [35] C. Deng, W. Chen, Z. Zhang, Y. Li, and Z. Feng, "Generation of OAM radio waves using circular vivaldi antenna array," *International Journal of Antennas and Propagation*, vol. 2013, no. 2, pp. 607–610, 2013.
- [36] X. Bai, X. Liang, R. Jin, and J. Geng, "Generation of OAM radio waves with three polarizations using circular horn antenna array," *2015 9th European Conference on Antennas and Propagation (EuCAP)*, pp. 1–4, April 2015.
- [37] R. Gaffoglio, A. Cagliero, A. D. Vita, and B. Sacco, "OAM multiple transmission using uniform circular arrays: Numerical modeling and experimental verification with two digital television signals," *Radio Sci.*, vol. 51, no. 6, pp. 645–658, June 2016.
- [38] Q. Bai, A. Tennant, B. Allen, and M. U. Rehman, "Generation of orbital angular momentum (OAM) radio beams with phased patch array," *2013 Loughborough Antennas Propagation Conference (LAPC)*, pp. 410–413, Nov 2013.
- [39] S. Xuehong, D. Yu, F. Yutang, and S. Muge, "The design of array antenna based on multi-modal OAM vortex electromagnetic wave," *2016 Progress in Electromagnetic Research Symposium (PIERS)*, pp. 2786–2791, Aug 2016.
- [40] M. Lin, Y. Gao, P. Liu, and J. Liu, "Theoretical analyses and design of circular array to generate orbital angular momentum," *IEEE Trans. Antennas Propag.*, vol. 65, no. 7, pp. 3510–3519, 2017.
- [41] A. Tennant and B. Allen, "Generation of radio frequency OAM radiation modes using circular time-switched and phased array antennas," in *Antennas and Propagation Conference*, 2012, pp. 1–4.
- [42] M. L. N. Chen, L. J. Jiang, and W. E. I. Sha, "Artificial perfect electric conductor-perfect magnetic conductor anisotropic metasurface for generating orbital angular momentum of microwave with nearly perfect conversion efficiency," *J. Appl. Phys.*, vol. 119, no. 6, p. 064506, 2016.
- [43] S. Yu, L. Li, G. Shi, C. Zhu, X. Zhou, and Y. Shi, "Design, fabrication, and measurement of reflective metasurface for orbital angular momentum vortex wave in radio frequency domain," *Appl. Phys. Lett.*, vol. 108, no. 12, p. 121903, 2016.
- [44] S. Yu, L. Li, G. Shi, C. Zhu, and Y. Shi, "Generating multiple orbital angular momentum vortex beams using a metasurface in radio frequency domain," *Appl. Phys. Lett.*, vol. 108, no. 24, p. 241901, 2016.
- [45] S. Yu, L. Li, and G. Shi, "Dual-polarization and dual-mode orbital angular momentum radio vortex beam generated by using reflective metasurface," *Appl. Phys. Express*, vol. 9, no. 8, p. 082202, 2016.
- [46] Y. Zhang, L. Yang, H. Wang, X. Zhang, and X. Jin, "Transforming surface wave to propagating OAM vortex wave via flat dispersive metasurface in radio frequency," *IEEE Antennas Wireless Propag. Lett.*, vol. 17, no. 1, pp. 172–175, 2018.
- [47] N. Kou, S. Yu, and L. Li, "Generation of high-order bessell vortex beam carrying orbital angular momentum using multilayer amplitude-phase-modulated surfaces in radiofrequency domain," *Applied Physics Express*, vol. 10, no. 1, p. 10617, 2016.
- [48] S. MacCalli, G. Pisano, S. Colafrancesco, B. Maffei, M. W. Ng, and M. Gray, "Q-plate for millimeter-wave orbital angular momentum manipulation," *Appl. Opt.*, vol. 52, no. 4, pp. 635–639, 2013.
- [49] R. Wunenburger, J. I. V. Lozano, and E. Brasselet, "Acoustic orbital angular momentum transfer to matter by chiral scattering," *New Journal of Physics*, vol. 17, no. 10, p. 103022, 2015.
- [50] S. Gspan, A. Meyer, S. Bernet, and M. Ritschmarte, "Optoacoustic generation of a helicoidal ultrasonic beam," *J. Acoust. Soc. Am.*, vol. 115, no. 3, pp. 1142–1146, 2004.
- [51] B. T. Hefner and P. L. Marston, "Acoustical helicoidal waves and laguerre-gaussian beams: Applications to scattering and to angular momentum transport," *J. Acoust. Soc. Am.*, vol. 103, no. 5, pp. 2971–2971, 1998.
- [52] J. Ealo, J. Prieto, and F. Seco, "Airborne ultrasonic vortex generation using flexible ferroelectrets," *IEEE T. Ultrason. Ferr.*, vol. 58, no. 8, pp. 1651–1657, 2011.
- [53] Y. Li, G. Guo, Q. Ma, J. Tu, and D. Zhang, "Deep-level stereoscopic multiple traps of acoustic vortices," *J. Appl. Phys.*, vol. 121, no. 16, p. 164901, 2017.
- [54] R. Marchiano and J. L. Thomas, "Synthesis and analysis of linear and nonlinear acoustical vortices," *Physical Review E Statistical Nonlinear and Soft Matter Physics*, vol. 71, no. 6, p. 066616, 2005.
- [55] K. Volke-Sepulveda, A. O. Santilln, and R. R. Boullosa, "Transfer of angular momentum to matter from acoustical vortices in free space," *Phys. Rev. Lett.*, vol. 100, no. 2, p. 024302, 2008.
- [56] L. Yang, Q. Ma, J. Tu, and D. Zhang, "Phase-coded approach for controllable generation of acoustical vortices," *J. Appl. Phys.*, vol. 113, no. 15, p. 154904, 2013.
- [57] T. Wang, M. Ke, W. Li, Q. Yang, C. Qiu, and Z. Liu, "Particle manipulation with acoustic vortex beam induced by a brass plate with spiral shape structure," *Appl. Phys. Lett.*, vol. 109, no. 12, p. 123506, 2016.
- [58] N. Jimnez, R. Pic, V. Snchez-morcillo, V. Romerogarcía, L. M. Garcíaraffi, and K. Staliunas, "Formation of high-order acoustic bessell beams by spiral diffraction gratings," *Phys. Rev. E*, vol. 94, no. 5, p. 053004, 2016.
- [59] N. Jimenez, V. Romerogarcía, L. M. Garcíaraffi, F. Camarena, and K. Staliunas, "Sharp acoustic vortex focusing by fresnel-spiral zone plates," *Appl. Phys. Lett.*, vol. 112, no. 20, p. 204101, 2018.
- [60] X. Jiang, J. Zhao, S. Liu, B. Liang, X. Zou, J. Yang, C. W. Qiu, and J. Cheng, "Broadband and stable acoustic vortex emitter with multi-arm coiling slits," *Appl. Phys. Lett.*, vol. 108, no. 20, p. 165, 2016.
- [61] R. D. Muelas-Hurtado, J. L. Ealo, J. F. Pazos-Ospina, and K. Volke-Sepulveda, "Generation of multiple vortex beam by means of active diffraction gratings," *Appl. Phys. Lett.*, vol. 112, no. 8, p. 084101, 2018.
- [62] X. Jiang, Y. Li, B. Liang, J. C. Cheng, and L. Zhang, "Convert acoustic resonances to orbital angular momentum," *Phys. Rev. Lett.*, vol. 117, no. 3, p. 034301, 2016.
- [63] L. Ye, C. Qiu, J. Lu, K. Tang, H. Jia, M. Ke, S. Peng, and Z. Liu, "Making sound vortices by metasurfaces," *Aip Advances*, vol. 6, no. 8, pp. 1734–337, 2016.
- [64] H. Esfahlani, H. Lissek, and J. R. Mosig, "Generation of acoustic helical wavefronts using metasurfaces," *Phys. Rev. B*, vol. 95, no. 2, p. 024312, 2017.
- [65] J. Leach, M. J. Padgett, S. M. Barnett, S. Frankearnold, and J. Courtial, "Measuring the orbital angular momentum of a single photon," *Phys. Rev. Lett.*, vol. 88, no. 1, p. 257901, 2002.
- [66] A. Mair, A. Vaziri, G. Weihs, and A. Zeilinger, "Entanglement of the orbital angular momentum states of photons," *Nature*, vol. 412, no. 6844, pp. 313–316, 2001.
- [67] G. Gibson, J. Courtial, M. Vasnetsov, M. J. Padgett, S. Frankearnold, S. M. Barnett, and V. PasKo, "Free-space information transfer using light beams carrying orbital angular momentum," *Opt. Express*, vol. 12, no. 22, pp. 5448–5456, 2004.
- [68] G. Gibson, J. Courtial, M. Vasnetsov, S. Barnett, S. Frankearnold, and M. Padgett, "Increasing the data density of free-space optical communications using orbital angular momentum," in *SPIE International Symposium on Optical Science and Technology*, 2004, pp. 367–373.
- [69] N. Zhang, X. C. Yuan, and R. E. Burge, "Extending the detection range of optical vortices by dammann vortex gratings," *Opt. Lett.*, vol. 35, no. 20, p. 3495, 2010.
- [70] C. Gao, S. Zhang, S. Fu, and T. Wang, "Integrating 55 dammann gratings to detect orbital angular momentum states of beams with the range of -24 to +24," *Appl. Opt.*, vol. 55, no. 7, p. 1514, 2016.
- [71] C. Kai, P. Huang, F. Shen, H. Zhou, and Z. Guo, "Orbital angular momentum shift keying based optical communication system," *IEEE Photonics Journal*, vol. 9, no. 2, pp. 1–10, 2017.
- [72] J. Lin, X. Yuan, S. Tao, and R. E. Burge, "Synthesis of multiple collinear helical modes generated by a phase-only element," *Journal of the Optical Society of America A Optics Image Science and Vision*, vol. 23, no. 5, pp. 1214–8, 2006.
- [73] H. I. Sztul and R. R. Alfano, "Double-slit interference with laguerre-gaussian beams," *Opt. Lett.*, vol. 31, no. 7, pp. 999–1001, 2006.
- [74] H. Zhou, L. Shi, X. Zhang, and J. Dong, "Dynamic interferometry measurement of orbital angular momentum of light," *Opt. Lett.*, vol. 39, no. 20, pp. 6058–61, 2014.
- [75] G. C. Berkhout and M. W. Beijersbergen, "Method for probing the orbital angular momentum of optical vortices in electromagnetic waves from astronomical objects," *Phys. Rev. Lett.*, vol. 101, no. 10, p. 100801, 2008.



- [76] C. S. Guo, L. L. Lu, and H. T. Wang, "Characterizing topological charge of optical vortices by using an annular aperture," *Opt. Lett.*, vol. 34, no. 23, p. 3686, 2009.
- [77] J. Leach, J. Courtial, K. Skeldon, S. M. Barnett, S. Franke-Arnold, and M. J. Padgett, "Interferometric methods to measure orbital and spin, or the total angular momentum of a single photon," *Phys. Rev. Lett.*, vol. 92, no. 1, p. 013601, 2004.
- [78] G. C. Berkhout, M. P. Lavery, J. Courtial, M. W. Beijersbergen, and M. J. Padgett, "Efficient sorting of orbital angular momentum states of light," *Phys. Rev. Lett.*, vol. 105, no. 15, p. 153601, 2010.
- [79] M. P. J. Lavery, D. J. Robertson, G. C. G. Berkhout, G. D. Love, M. J. Padgett, and J. Courtial, "Refractive elements for the measurement of the orbital angular momentum of a single photon," *Opt. Express*, vol. 20, no. 3, pp. 2110–5, 2012.
- [80] M. Mirhosseini, M. Malik, Z. Shi, and R. W. Boyd, "Efficient separation of the orbital angular momentum eigenstates of light," *Nature Commun.*, vol. 4, no. 7, p. 2781, 2013.
- [81] E. Karimi, B. Piccirillo, E. Nagali, L. Marrucci, and E. Santamato, "Efficient generation and sorting of orbital angular momentum eigenmodes of light by thermally tuned q-plates," *Appl. Phys. Lett.*, vol. 94, no. 23, p. 299, 2009.
- [82] P. Jia, Y. Yang, and X. Yuan, "Sidelobe-modulated optical vortices for free-space communication," *Opt. Lett.*, vol. 38, no. 4, pp. 588–90, 2013.
- [83] J. Long, R. Liu, F. Wang, Y. Wang, P. Zhang, H. Gao, and F. Li, "Evaluating laguerre-gaussian beams with an invariant parameter," *Opt. Lett.*, vol. 38, no. 16, pp. 3047–3049, 2013.
- [84] C. R. Doerr, L. Buhl, and N. K. Fontaine, "Efficient multiplexing and demultiplexing of free-space orbital angular momentum using photonic integrated circuits," in *Optical Fiber Communication Conference and Exposition*, 2012, pp. 1–3.
- [85] T. Su, R. P. Scott, S. S. Djordjevic, N. K. Fontaine, D. J. Geisler, X. Cai, and S. J. Yoo, "Demonstration of free space coherent optical communication using integrated silicon photonic orbital angular momentum devices," *Opt. Express*, vol. 20, no. 9, pp. 9396–9402, 2012.
- [86] S. M. Mohammadi, L. K. S. Daldorff, K. Forozesh, T. Bo, J. E. S. Bergman, B. Isham, R. Karlsson, and T. D. Carozzi, "Orbital angular momentum in radio: Measurement methods," *Radio Sci.*, vol. 45, no. 4, pp. –, 2010.
- [87] Y. Hu, S. Zheng, Z. Zhang, H. Chi, X. Jin, and X. Zhang, "Simulation of orbital angular momentum radio communication systems based on partial aperture sampling receiving scheme," *IET Microwaves Antennas and Propagation*, vol. 10, no. 10, pp. 1043–1047, 2016.
- [88] M. Xie, X. Gao, M. Zhao, W. Zhai, W. Xu, J. Qian, M. Lei, and S. Huang, "Mode measurement of a dual-mode radio frequency orbital angular momentum beam by circular phase gradient method," *IEEE Antennas Wireless Propag. Lett.*, vol. PP, no. 99, pp. 1–1, 2017.
- [89] H. Wu, Y. Yuan, Z. Zhang, and C. Ji, "UCA-based orbital angular momentum radio beam generation and reception under different array configurations," in *Sixth International Conference on Wireless Communications and Signal Processing*, 2014, pp. 1–6.
- [90] S. Zheng, X. Hui, J. Zhu, H. Chi, X. Jin, S. Yu, and X. Zhang, "Orbital angular momentum mode-demultiplexing scheme with partial angular receiving aperture," *Opt. Express*, vol. 23, no. 9, pp. 12 251–7, 2015.
- [91] C. Shi, M. Dubois, Y. Wang, and X. Zhang, "High-speed acoustic communication by multiplexing orbital angular momentum," *Proc Natl Acad Sci U S A*, vol. 114, no. 28, pp. 7250–7253, 2017.
- [92] X. Jiang, B. Liang, J. Cheng, and C. Qiu, "Twisted acoustics: Metasurface-enabled multiplexing and demultiplexing," *Advanced Materials*, vol. 30, no. 18, p. 1800257, 2018.
- [93] Y. Ren, Z. Wang, P. Liao, L. Li, G. Xie, H. Huang, Z. Zhao, and Y. Yan, "Experimental characterization of a 400gb/s orbital angular momentum multiplexed free-space optical link over 120-meters," *Opt. Lett.*, vol. 41, no. 3, pp. 622–625, 2016.
- [94] M. Krenn, R. Fickler, M. Fink, J. Handsteiner, M. Malik, T. Scheidl, R. Ursin, and A. Zeilinger, "Communication with spatially modulated light through turbulent air across vienna," *New Journal of Physics*, vol. 16, 2014.
- [95] M. Krenn, J. Handsteiner, M. Fink, R. Fickler, R. Ursin, M. Malik, and A. Zeilinger, "Twisted light transmission over 143 km," *Proc. Natl. Acad. Sci. U. S. A.*, vol. 113, no. 48, p. 13648, 2016.
- [96] J. Lin, X. Yuan, S. Tao, and R. E. Burge, "Multiplexing free-space optical signals using superimposed collinear orbital angular momentum states," *Appl. Opt.*, vol. 46, no. 21, pp. 4680–4685, 2007.
- [97] Z. Li, X. Gu, and L. Wang, "High-dimensional free-space optical communications based on orbital angular momentum coding," *Opt. Commun.*, vol. 410, no. 7, pp. 333–337, 2018.
- [98] J. Wang, J. Y. Yang, I. M. Fazal, N. Ahmed, Y. Yan, H. Huang, Y. Ren, Y. Yue, S. Dolinar, and M. Tur, "Terabit free-space data transmission employing orbital angular momentum multiplexing," *Nature Photonics*, vol. 6, no. 7, pp. 488–496, 2012.
- [99] H. Huang, G. Xie, Y. Yan, N. Ahmed, Y. Ren, Y. Yue, D. Rogawski, M. J. Willner, B. I. Erkmen, and K. M. Birnbaum, "100 tbit/s free-space data link enabled by three-dimensional multiplexing of orbital angular momentum, polarization, and wavelength," *Opt. Lett.*, vol. 39, no. 2, p. 197, 2014.
- [100] J. Wang, S. Li, M. Luo, and J. Liu, "N-dimensional multiplexing link with 1.036-pbit/s transmission capacity and 112.6-bit/s/hz spectral efficiency using ofdm-8qam signals over 368 wdm pol-muxed 26 OAM modes," in *European Conference on Optical Communication*, 2014, pp. 1–3.
- [101] T. Abderrahmen, R. G. Carmelo, D. Angela, N. Bienvenu, B. S. Amine, Z. Mourad, and F. Andrew, "Optical communication beyond orbital angular momentum," *Scientific Reports*, vol. 6, p. 27674, 2016.
- [102] G. Xie, Y. Ren, Y. Yan, H. Huang, N. Ahmed, L. Li, Z. Zhao, C. Bao, M. Tur, and S. Ashrafi, "Experimental demonstration of a 200-gbit/s free-space optical link by multiplexing laguerre-gaussian beams with different radial indices," *Opt. Lett.*, vol. 41, no. 15, p. 3447, 2016.
- [103] J. Du and J. Wang, "High-dimensional structured light coding/decoding for free-space optical communications free of obstructions," *Opt. Lett.*, vol. 40, no. 21, pp. 4827–30, 2015.
- [104] N. Ahmed, Z. Zhe, L. Long, H. Hao, M. P. J. Lavery, P. Liao, Y. Yan, W. Zhe, G. Xie, and Y. Ren, "Mode-division-multiplexing of multiple bessell-gaussian beams carrying orbital-angular-momentum for obstruction-tolerant free-space optical and millimetre-wave communication links," *Scientific Reports*, vol. 6, p. 22082, 2016.
- [105] F. Zhu, S. Huang, W. Shao, J. Zhang, M. Chen, W. Zhang, and J. Zeng, "Free-space optical communication link using perfect vortex beams carrying orbital angular momentum (OAM)," *Opt. Commun.*, vol. 396, pp. 50–57, 2017.
- [106] A. E. Willner, A. F. Molisch, G. Xie, H. Huang, L. Li, M. P. J. Lavery, M. Tur, N. Ashrafi, N. Ahmed, and R. Bock, "Performance metrics and design considerations for a free-space optical orbital-angular-momentum-multiplexed communication link," *Optica*, vol. 2, no. 4, p. 357, 2015.
- [107] Y. Ren, H. Huang, G. Xie, N. Ahmed, Y. Yan, B. I. Erkmen, N. Chandrasekaran, M. P. Lavery, N. K. Steinhoff, and M. Tur, "Atmospheric turbulence effects on the performance of a free space optical link employing orbital angular momentum multiplexing," *Opt. Lett.*, vol. 38, no. 20, p. 4062, 2013.
- [108] C. Paterson, "Atmospheric turbulence and orbital angular momentum of single photons for optical communication," *Phys. Rev. Lett.*, vol. 94, no. 15, p. 153901, 2005.
- [109] G. A. Tyler and R. W. Boyd, "Influence of atmospheric turbulence on the propagation of quantum states of light carrying orbital angular momentum," *Opt. Lett.*, vol. 34, no. 2, pp. 142–144, 2009.
- [110] R. Brandon, P. J. L. Martin, M. Mehul, N. O. Malcolm, M. Mohammad, J. R. David, P. Miles, and W. B. Robert, "Influence of atmospheric turbulence on states of light carrying orbital angular momentum," *Opt. Lett.*, vol. 37, no. 17, pp. 3735–3737, 2012.
- [111] S. Li, S. Chen, C. Gao, A. E. Willner, and J. Wang, "Atmospheric turbulence compensation in orbital angular momentum communications: Advances and perspectives," *Opt. Commun.*, vol. 408, 2018.
- [112] B. Zhu, T. F. Taunay, M. Fishteyn, X. Liu, S. Chandrasekhar, M. F. Yan, J. M. Fini, E. M. Monberg, and F. V. Dimarcello, "112-tb/s space-division multiplexed dwdm transmission with 14-b/s/hz aggregate spectral efficiency over a 76.8-km seven-core fiber," *Opt. Express*, vol. 19, no. 17, pp. 16 665–16 671, 2011.
- [113] J. Sakaguchi, Y. Awaji, N. Wada, A. Kanno, T. Kawanishi, T. Hayashi, T. Taru, T. Kobayashi, and M. Watanabe, "Space division multiplexed transmission of 109-tb/s data signals using homogeneous seven-core fiber," *J. Lightw. Technol.*, vol. 30, no. 4, pp. 658–665, 2012.
- [114] S. Randel, R. Ryf, A. Sierra, P. J. Winzer, A. H. Gnauck, C. A. Bolle, R. J. Essiambre, D. W. Peckham, A. McCurdy, and L. R. Jr, "6x56-gb/s mode-division multiplexed transmission over 33-km few-mode fiber enabled by 6x6 mimo equalization," *Opt. Express*, vol. 19, no. 17, pp. 16 697–707, 2011.
- [115] N. Bozinovic, P. Kristensen, S. Ramachandran, and S. Golowich, "Control of orbital angular momentum of light with optical fibers," *Opt. Lett.*, vol. 37, no. 13, p. 2451, 2012.
- [116] N. Bozinovic, P. Kristensen, and S. Ramachandran, "Long-range fiber-transmission of photons with orbital angular momentum," in *Lasers and Electro-Optics*, 2011, pp. 1–2.

- [117] N. Bozinovic, Y. Yue, Y. Ren, M. Tur, P. Kristensen, H. Huang, A. E. Willner, and S. Ramachandran, "Terabit-scale orbital angular momentum mode division multiplexing in fibers," *Science*, vol. 340, no. 6140, pp. 1545–1548, 2013.
- [118] Y. Yue, Y. Yan, N. Ahmed, J. Y. Yang, L. Zhang, Y. Ren, H. Huang, S. Dolinar, M. Tur, and A. Willner, "Mode and propagation effects of optical orbital angular momentum (OAM) modes in a ring fiber," *IEEE Photonics Journal*, vol. 4, no. 2, pp. 535–543, 2012.
- [119] S. Li and J. Wang, "Multi-orbital-angular-momentum multi-ring fiber for high-density space-division multiplexing," *IEEE Photonics Journal*, vol. 5, no. 5, pp. 7 101 007–7 101 007, 2013.
- [120] H. Zhang, W. Zhang, L. Xi, X. Tang, X. Zhang, and X. Zhang, "A new type circular photonic crystal fiber for orbital angular momentum mode transmission," *IEEE Photon. Technol. Lett.*, vol. 28, no. 13, pp. 1426–1429, 2016.
- [121] G. Zhou, G. Zhou, C. Chen, M. N. Xu, C. Xia, and Z. Hou, "Design and analysis of a microstructure ring fiber for orbital angular momentum transmission," *IEEE Photonics Journal*, vol. 8, no. 2, pp. 1–12, 2016.
- [122] X. Zeng, Y. Li, Q. Mo, W. Li, Y. Tian, Z. Liu, and J. Wu, "Experimental investigation of  $lp_{11}$  mode to OAM conversion in few mode-polarization maintaining fiber and the usage for all fiber OAM generator," *IEEE Photonics Journal*, vol. 8, no. 4, pp. 1–7, 2016.
- [123] Y. Li, L. Jin, H. Wu, S. Gao, Y. H. Feng, and Z. Li, "Superposing multiple  $lp$  modes with micro phase difference distributed along fiber to generate OAM mode," *IEEE Photonics Journal*, vol. 9, no. 2, pp. 1–9, 2017.
- [124] S. Li, Z. Xu, R. Zhao, L. Shen, C. Du, and J. Wang, "Generation of orbital angular momentum beam using fiber-to-fiber butt coupling," *IEEE Photonics Journal*, vol. 10, no. 4, pp. 1–7, 2018.
- [125] S. Chen and J. Wang, "Characterization of red/green/blue orbital angular momentum modes in conventional g.652 fiber," *IEEE J. Quantum Electron.*, vol. 53, no. 4, pp. 1–14, 2017.
- [126] F. E. Mahmoudi and S. D. Walker, "4-gbps uncompressed video transmission over a 60-ghz orbital angular momentum wireless channel," *IEEE Wireless Commun. Lett.*, vol. 2, no. 2, pp. 223–226, 2013.
- [127] B. Allen, A. Tennant, Q. Bai, and E. Chatziantoniou, "Wireless data encoding and decoding using OAM modes," *Electronics Letters*, vol. 50, no. 3, pp. 232–233, 2014.
- [128] Y. Yan, G. Xie, M. P. Lavery, H. Huang, N. Ahmed, C. Bao, Y. Ren, Y. Cao, L. Li, and Z. Zhao, "High-capacity millimeter-wave communications with orbital angular momentum multiplexing," *Nature Commun.*, vol. 5, p. 4876, 2014.
- [129] Y. Yan, L. Li, Z. Zhao, G. Xie, Z. Wang, Y. Ren, N. Ahmed, S. Sajuyigbe, S. Talwar, and M. Tur, "32-gbit/s 60-ghz millimeter-wave wireless communication using orbital angular momentum and polarization multiplexing," in *IEEE International Conference on Communications*, 2016, pp. 1–6.
- [130] Z. Zhao, Y. Yan, L. Li, G. Xie, Y. Ren, N. Ahmed, Z. Wang, C. Liu, A. J. Willner, and P. Song, "A dual-channel 60 ghz communications link using patch antenna arrays to generate data-carrying orbital-angular-momentum beams," in *IEEE International Conference on Communications*, 2016, pp. 1–6.
- [131] X. Hui, S. Zheng, Y. Chen, Y. Hu, X. Jin, H. Chi, and X. Zhang, "Multiplexed millimeter wave communication with dual orbital angular momentum (OAM) mode antennas," *Scientific Reports*, vol. 5, p. 10148, 2015.
- [132] Z. Zhao, Y. Ren, G. Xie, Y. Yan, L. Li, H. Huang, C. Bao, N. Ahmed, M. P. Lavery, C. Zhang, N. Ashrafi, S. Ashrafi, S. Talwar, S. Sajuyigbe, M. Tur, A. F. Molisch, and A. E. Willner, "Experimental demonstration of 16-gbit/s millimeter-wave communications link using thin metamaterial plates to generate data-carrying orbital-angular-momentum beams," in *2015 IEEE International Conference on Communications (ICC)*, June 2015, pp. 1392–1397.
- [133] W. Zhang, S. Zheng, X. Hui, R. Dong, X. Jin, H. Chi, and X. Zhang, "Mode division multiplexing communication using microwave orbital angular momentum: An experimental study," *IEEE Trans. Wireless Commun.*, vol. 16, no. 2, pp. 1308–1318, Feb 2017.
- [134] O. Edfors and A. J. Johansson, "Is orbital angular momentum (OAM) based radio communication an unexploited area?" *IEEE Trans. Antennas Propag.*, vol. 60, no. 2, pp. 1126–1131, 2012.
- [135] M. Tamagnone, C. Craeye, and J. Perruisseau-Carrier, "Comment on 'encoding many channels on the same frequency through radio vorticity: first experimental test'," *New Journal of Physics*, no. 14, p. 118001, 2012.
- [136] R. Chen, H. Xu, W. Yang, and J. Li, "On the performance of OAM in keyhole channels," *IEEE Wireless Commun. Lett.*, pp. 1–4, 2018.
- [137] M. Oldoni, F. Spinello, E. Mari, G. Parisi, C. G. Smeda, F. Tamburini, F. Romanato, R. A. Ravanelli, P. Coassini, and B. Thid, "Space-division demultiplexing in orbital-angular-momentum-based mimo radio systems," *IEEE Trans. Antennas Propag.*, vol. 63, no. 10, pp. 4582–4587, Oct 2015.
- [138] Z. Zhang, S. Zheng, Y. Chen, X. Jin, H. Chi, and X. Zhang, "The capacity gain of orbital angular momentum based multiple-input-multiple-output system," *Scientific Reports*, no. 6, p. 25418, 2016.
- [139] X. Ge, R. Zi, X. Xiong, Q. Li, and L. Wang, "Millimeter wave communications with OAM-sm scheme for future mobile networks," *IEEE J. Sel. Areas Commun.*, vol. 35, no. 9, pp. 2163–2177, Sept 2017.
- [140] Y. Ren, L. Li, G. Xie, Y. Yan, Y. Cao, H. Huang, N. Ahemd, M. J. Lavery, Z. Zhao, C. Zhang, M. Tur, M. Padgett, G. Caire, A. F. Molisch, and A. E. Willner, "Experimental demonstration of 16 gbit/s millimeter-wave communications using mimo processing of 2 OAM modes on each of two transmitter/receiver antenna apertures," in *2014 IEEE Global Communications Conference*, Dec 2014, pp. 3821–3826.
- [141] Y. Ren, L. Li, G. Xie, Y. Yan, Y. Cao, H. Huang, N. Ahmed, Z. Zhao, P. Liao, C. Zhang, G. Caire, A. F. Molisch, M. Tur, and A. E. Willner, "Line-of-sight millimeter-wave communications using orbital angular momentum multiplexing combined with conventional spatial multiplexing," *IEEE Trans. Wireless Commun.*, vol. 16, no. 5, pp. 3151–3161, May 2017.
- [142] Y. Ren, Z. Wang, G. Xie, L. Li, Y. Cao, C. Liu, P. Liao, Y. Yan, N. Ahmed, and Z. Zhao, "Free-space optical communications using orbital-angular-momentum multiplexing combined with mimo-based spatial multiplexing," *Opt. Lett.*, vol. 40, no. 18, pp. 4210–4213, 2015.
- [143] R. Chen, H. Xu, M. Moretti, and J. Li, "Beam steering for the misalignment in UCA-based OAM communication systems," *IEEE Wireless Commun. Lett.*, vol. 7, no. 4, pp. 582–585, Aug 2018.
- [144] Y. Yan, L. Li, G. Xie, C. Bao, P. Liao, H. Huang, Y. Ren, N. Ahmed, Z. Zhao, M. P. Lavery, N. Ashrafi, S. Ashrafi, S. Talwar, S. Sajuyigbe, M. Tur, A. F. Molisch, and A. E. Willner, "Experimental measurements of multipath-induced intra- and inter-channel crosstalk effects in a millimeter-wave communications link using orbital-angular-momentum multiplexing," in *2015 IEEE International Conference on Communications (ICC)*, June 2015, pp. 1370–1375.
- [145] Y. Yan, L. Li, G. Xie, C. Bao, P. Liao, H. Huang, Y. Ren, N. Ahmed, Z. Zhao, and Z. Wang, "Multipath effects in millimetre-wave wireless communication using orbital angular momentum multiplexing," *Scientific Reports*, vol. 6, p. 33482, 2016.
- [146] R. Chen, W. Yang, H. Xu, and J. Li, "A 2-d fft-based transceiver architecture for OAM-OFDM systems with UCA antennas," *IEEE Trans. Veh. Technol.*, vol. 67, no. 6, pp. 5481–5485, June 2018.
- [147] A. Ashkin, J. M. Dziedzic, J. E. Bjorkholm, and S. Chu, "Observation of a single-beam gradient force optical trap for dielectric particles," *Opt. Lett.*, vol. 11, no. 5, p. 288, 1986.
- [148] H. He, M. E. Friese, N. R. Heckenberg, and H. Rubinsztein-Dunlop, "Direct observation of transfer of angular momentum to absorptive particles from a laser beam with a phase singularity," *Phys. Rev. Lett.*, vol. 75, no. 5, pp. 826–829, 1995.
- [149] N. B. Simpson, K. Dholakia, L. Allen, and M. J. Padgett, "Mechanical equivalence of spin and orbital angular momentum of light: an optical spanner," *Opt. Lett.*, vol. 22, no. 1, pp. 52–54, 1997.
- [150] M. E. Friese, J. Enger, H. Rubinsztein-Dunlop, and N. R. Heckenberg, "Optical angular-momentum transfer to trapped absorbing particles," *Physical Review A*, vol. 54, no. 2, p. 1593, 1996.
- [151] A. T. O'Neil, I. Macvicar, L. Allen, and M. J. Padgett, "Intrinsic and extrinsic nature of the orbital angular momentum of a light beam," *Phys. Rev. Lett.*, vol. 88, no. 5, p. 053601, 2002.
- [152] V. Garcés-Chávez, D. McGloin, M. J. Padgett, W. Dultz, H. Schmitzer, and K. Dholakia, "Observation of the transfer of the local angular momentum density of a multiringed light beam to an optically trapped particle," *Phys. Rev. Lett.*, vol. 91, no. 9, p. 093602, 2003.
- [153] C. R. P. Courtney, B. W. Drinkwater, C. E. M. Demore, and S. Cochran, "Dexterous manipulation of microparticles using bessel-function acoustic pressure fields," *Appl. Phys. Lett.*, vol. 102, no. 12, p. 123508, 2013.
- [154] C. R. P. Courtney, C. E. M. Demore, H. Wu, A. Grinenko, P. D. Wilcox, S. Cochran, and B. W. Drinkwater, "Independent trapping and manipulation of microparticles using dexterous acoustic tweezers," *Appl. Phys. Lett.*, vol. 104, no. 15, pp. 492–660, 2014.
- [155] A. Anhäuser, R. Wunenburger, and E. Brasselet, "Acoustic rotational manipulation using orbital angular momentum transfer," *Phys. Rev. Lett.*, vol. 109, no. 3, p. 034301, 2012.
- [156] S. W. Hell and J. Wichmann, "Breaking the diffraction resolution limit by stimulated emission: stimulated-emission-depletion fluorescence microscopy," *Opt. Lett.*, vol. 19, no. 11, pp. 780–782, 1994.

- [157] L. Li and F. Li, "Beating the rayleigh limit: orbital-angular-momentum-based super-resolution diffraction tomography," *Phys. Rev. E*, vol. 88, no. 3, p. 033205, 2013.
- [158] C. Maurer, A. Jesacher, S. Bernet, and M. Ritsch-Marte, "What spatial light modulators can do for optical microscopy," *Laser and Photonics Reviews*, vol. 5, no. 1, pp. 81–101, 2011.
- [159] G. A. Swartzlander, "Peering into darkness with a vortex spatial filter," *Opt. Lett.*, vol. 26, no. 8, pp. 497–499, 2001.
- [160] G. A. Swartzlander, E. L. Ford, R. S. Abdul-Malik, L. M. Close, M. A. Peters, D. M. Palacios, and D. W. Wilson, "Astronomical demonstration of an optical vortex coronagraph," *Opt. Express*, vol. 16, no. 14, pp. 10 200–10 207, 2008.
- [161] S. Fühapter, A. Jesacher, S. Bernet, and M. Ritsch-Marte, "Spiral phase contrast imaging in microscopy," *Opt. Express*, vol. 13, no. 3, pp. 689–694, 2005.
- [162] J. Wang, W. Zhang, Q. Qi, S. Zheng, and L. Chen, "Gradual edge enhancement in spiral phase contrast imaging with fractional vortex filters," *Scientific Reports*, vol. 5, p. 15826, 2015.
- [163] S. Fühapter, A. Jesacher, S. Bernet, and M. Ritschmarte, "Spiral interferometry," *Opt. Lett.*, vol. 30, no. 15, pp. 1953–1955, 2005.
- [164] K. Liu, Y. Cheng, Z. Yang, H. Wang, Y. Qin, and X. Li, "Orbital-angular-momentum-based electromagnetic vortex imaging," *IEEE Antennas Wireless Propag. Lett.*, vol. 14, pp. 711–714, 2015.
- [165] K. Liu, Y. Cheng, Y. Gao, X. Li, Y. Qin, and H. Wang, "Super-resolution radar imaging based on experimental OAM beams," *Appl. Phys. Lett.*, vol. 110, no. 16, p. 033001, 2017.
- [166] G. Guo, H. U. Weidong, and D. U. Xiaoyong, "Electromagnetic vortex based radar target imaging," *Journal of National University of Defense Technology*, 2013.
- [167] C. Zhang and D. Chen, "Large-scale orbital angular momentum radar pulse generation with rotational antenna," *IEEE Antennas Wireless Propag. Lett.*, vol. 16, pp. 2316–2319, 2017.
- [168] X. Bu, Z. Zhang, L. Chen, X. Liang, H. Tang, and X. M. Wang, "Implementation of vortex electromagnetic waves high-resolution synthetic aperture radar imaging," *IEEE Antennas Wireless Propag. Lett.*, vol. 17, no. 5, pp. 764–767, 2018.
- [169] T. Yuan, H. Wang, Y. Qin, and Y. Cheng, "Electromagnetic vortex imaging using uniform concentric circular arrays," *IEEE Antennas Wireless Propag. Lett.*, vol. 15, pp. 1024–1027, 2016.
- [170] K. Liu, Y. Cheng, X. Li, Y. Qin, H. Wang, and Y. Jiang, "Generation of orbital angular momentum beams for electromagnetic vortex imaging," *IEEE Antennas Wireless Propag. Lett.*, vol. 15, pp. 1873–1876, 2016.
- [171] T. Yuan, Y. Cheng, H. Wang, and Y. Qin, "Beam steering for electromagnetic vortex imaging using uniform circular arrays," *IEEE Antennas Wireless Propag. Lett.*, vol. 16, pp. 704–707, 2017.
- [172] M. Lin, Y. Gao, P. Liu, and J. Liu, "Super-resolution orbital angular momentum based radar targets detection," *Electronics Letters*, vol. 52, no. 13, pp. 1168–1170, 2016.
- [173] —, "Improved OAM-based radar targets detection using uniform concentric circular arrays," *International Journal of Antennas and Propagation*, vol. 2016, no. 6, pp. 1–8, 2016.
- [174] R. Chen, W.-X. Long, Y. Gao, and J. Li, "Orbital angular momentum-based two-dimensional super-resolution targets imaging," in *2018 IEEE Global Conference on Signal and Information Processing (GlobalSIP)*, Nov 2018.
- [175] T. Yuan, H. Liu, Y. Cheng, Y. Qin, and H. Wang, "Orbital-angular-momentum-based electromagnetic vortex imaging by least-squares method," in *2016 IEEE International Geoscience and Remote Sensing Symposium (IGARSS)*, July 2016, pp. 6645–6648.